Chinese Journal of Chemical Engineering 90 (2026) 168–180

Contents lists available at ScienceDirect

Chinese Journal of Chemical Engineering

journal homepage: www.elsevier.com/locate/CJChE

Full Length Article

Knee point-guided heterogeneous surrogate-assisted optimization for multi-objective coal gasification system

Wenlu Li [1,2], Nan Guo [1], Tiewei Shang [1], Yueyang Sun [1], Dapeng Li [3], Xiaolong Gao [4], Wei Xiong [5], Junfei Qiao [1,*]

[1] Information Science Department, Beijing University of Technology, Beijing 100024, China
[2] College of Carbon Neutrality Future Technology, Beijing University of Technology, Beijing 100124, China
[3] School of Electrical Engineering, Liaoning University of Technology, Jinzhou 121001, China
[4] Baotou Reclaimed Water Resources and Sewage Treatment Co., Ltd., Baotou 014000, China
[5] Baotou Water Group, Baotou 014000, China

ARTICLE INFO

Article history:
Received 27 March 2025
Received in revised form
28 August 2025
Accepted 1 September 2025
Available online 22 November 2025

Keywords:
Coal gasification
Expensive multi-objective optimization
Kriging
Feedforward neural network (FNN)
Knee point
Model management

ABSTRACT

Coal gasification technology plays a pivotal role in chemical production as a key process for efficiently converting coal into liquid fuels and chemical feedstocks. During gasification, high-temperature reactions generate syngas, and optimizing its operational parameters is essential for improving syngas quality, carbon efficiency and liquid fuel yield. However, the intricate chemical reactions and heat transfer mechanisms in gasification necessitate costly simulations or experimental testing, making it an expensive multi-objective optimization problem. To address this challenge, this paper proposes a Knee Point-guided Heterogeneous Surrogate-assisted Evolutionary Algorithm (KG-HSEA) that integrates Kriging and Feedforward Neural Networks (FNN) to construct a heterogeneous surrogate model, leveraging their complementary strengths to reduce computational costs while maintaining predictive accuracy. By incorporating a knee point-guided search mechanism, the method prioritizes solutions that embody critical trade-offs among conflicting objectives. Moreover, an adaptive sampling strategy combined with dual-archive management is employed to dynamically update the surrogate model, ensuring it adapts to unstable operating conditions while maintaining robust convergence-diversity balance in coal gasification processes. Experimental results show that KG-HSEA achieved a 71.9% superiority rate with 23 optimal solutions out of 32 benchmark problems, highlighting its potential for efficient and feasible coal gasification optimization.

1. Introduction

The coal gasification process is a core component of coal-to-liquids (CTL) technology, where solid coal is converted into syngas, a crucial feedstock for producing methanol, ethylene glycol, and liquid fuels [1]. In real-world coal gasification operations, numerous practical challenges emerge. For instance, while enhancing the energy quality of syngas products is critical for efficient downstream processing, such improvements often come at the cost of increased energy consumption [2]. Similarly, maintaining the operation stability of the system under varying feedstock conditions and reaction environments is essential yet difficult to achieve [3]. These conflicting requirements range from syngas quality, gasification efficiency, and system energy consumption to highlight the intrinsic complexity of coal gasification optimization [4,5]. As a result, coal gasification optimization is typically formulated as a multi-objective optimization problem (MOP) [6]. In the complex mechanism analysis of the coal gasification system, Xie *et al.* [7] established a computational fluid dynamics (CFD) model to simulate the coal chemical looping gasification process in the fuel reactor (FR), while Huang *et al.* [8] carried out the CFD optimization design of the header of the supercritical water gasification heat exchanger. However, due to the high computational cost of evaluating objective functions, particularly when involving CFD simulations to model complex gasification reactions and multiphase flow behaviors [9], this optimization problem is more accurately classified as an expensive multi-objective optimization problem (EMOP). In EMOPs, the expensive evaluations of objective functions significantly increase computational expenses and extend solution timeframes, necessitating surrogate-assisted optimization methods to approximate these functions and reduce the computational burden [10].

* Corresponding author.
E-mail address: adqiao@bjut.edu.cn (J. Qiao).

https://doi.org/10.1016/j.cjche.2025.09.028

In response to the challenges posed by EMOPs in coal gasification systems, previous studies have applied traditional heuristic algorithms including swarm intelligence algorithms(SIAs) and evolutionary algorithms to coal gasification optimization. Although these approaches have achieved some success, they typically struggle with high computational costs and the difficulty of balancing multiple conflicting objectives under complex process conditions [11]. Consequently, surrogate-assisted optimization has emerged as a promising alternative, which can alleviate the burden of expensive function evaluations by approximating the objective functions [12]. These algorithms mitigate the computational burden of costly function evaluations by approximating the true objective functions, thereby enhancing the efficiency of the optimization process. Among them, Pan *et al.* [13] proposed a classification-based surrogate-assisted evolutionary algorithm (CSEA) using FNN models to pre-select promising solutions for re-evaluation. Tian *et al.* [14] introduced a probabilistic neural network-based surrogate model using pairwise comparisons. An adaptive Bayesian surrogate-assisted evolutionary algorithm (ABSAEA) was proposed by Wang *et al.* [15] which dynamically adjusts hyperparameters in the acquisition function to select candidate solutions evaluated by the original expensive function. The success of such algorithms relies on two essential components: the construction of the surrogate model and the updating of the optimization process.

To begin with, constructing an appropriate surrogate model is crucial for accurately capturing the complex and nonlinear behavior inherent in coal gasification systems. In general, surrogate models fall into two categories: neural network-based models and statistical models [16]. For instance, Hua *et al.* [17] proposed a convolutional neural network (CNN) process monitoring method based on dual channel pooling and homologous bilinear model to improve the operation effect of industrial coking furnace. Lughofer *et al.* [18] established a prediction and interpretation model for the three key process variables of hot metal temperature, silicon concentration and cooling capacity in the process of ironmaking blast furnace.

However, single surrogate models face limitations in handling diverse datasets or maintaining optimization performance, particularly in high-dimensional or highly nonlinear problems. While Kriging excels with small to medium-scale nonlinear data by minimizing structural risk and enhancing generalization [19,20], its performance degrades with larger datasets. In such cases, FNN with its strong function approximation capabilities can capture complex nonlinear relationships [21]. Compared to more complex networks that require large amounts of data and computing power, it demands less data, making it especially suitable for situations with limited samples.These two models exhibit complementary strengths when dealing with different types of data and problems.

Furthermore, it is critical to continuously update the surrogate model throughout the optimization process to ensure that the algorithm adapts to the evolving information [22]. This iterative refinement of the surrogate model allows the optimization to focus on the most promising regions of the solution space. Among dominance-based evolutionary algorithms, the Non-dominated Sorting Genetic Algorithm II (NSGA-II) has been widely successful in both theoretical and practical applications, it faces challenges when dealing with complex multi-objective optimization problems (MOPs), particularly in balancing population diversity and exploring the solution space. To address these limitations, several improved mechanisms have been proposed, such as the reference vector-guided evolutionary algorithm by Song *et al.* [23], which achieved promising results by enhancing population diversity. Another approach is to embed knee points in the selection mechanism, which can increase selection pressure, improve solution diversity, and guide the search towards key trade-off solutions [24]. Prioritizing knee points ensures that critical turning points on the PF are utilized, enhancing both the convergence and diversity of the solution set [25].

At present, it is essential to recognize that in the coal gasification system, datasets vary in scale and can be classified into small, medium, large, and very large types. Simultaneously, in the process of algorithm evolution, relying solely on traditional crowding distance to maintain diversity may result in suboptimal performance during the later stages of the search. Moreover, when there are highly nonlinear or complex trade-offs among multiple objectives, using reference vectors might fail to accurately capture these intricate points of compromise. In contrast, employing knee points to construct a guidance mechanism can more effectively handle such complex relationships. Additionally, this mechanism enhances the population's exploration ability, providing structured guidance to the solution space and overcoming the shortcomings of traditional methods in balancing diversity and local search.

To address expensive multi-objective optimization challenges in coal gasification systems. These systems involve high-temperature reactions, complex chemical kinetics, and intense heat transfer dynamics that create strongly coupled nonlinear interactions. This paper proposed a knee point-guided heterogeneous surrogate-assisted evolutionary algorithm (KG-HSEA). These complexities make it particularly difficult to simultaneously optimize system stability, energy efficiency, and syngas quality, which are essential for balanced operations. The main contributions are as follows:

(1) A heterogeneous surrogate-assisted framework is introduced by integrating Kriging and feedforward neural networks (FNN). This framework addresses the challenge of accurately modeling the complex and nonlinear behavior of coal gasification systems. By leveraging Kriging's local accuracy in low-dimensional settings and FNN's nonlinear fitting capabilities in high-dimensional environments, the framework enhances the precision and generalization of surrogate modeling, enabling more reliable predictions of syngas quality and system performance.
(2) A knee point-guided search mechanism is developed to prioritize solutions that represent balanced trade-offs among conflicting objectives. This approach improves the optimization of key coal gasification parameters by preventing convergence toward extreme values of any single objective.
(3) An adaptive sampling strategy based on dual-archive management is designed to dynamically adjust sample selection using both convergence and diversity indicators. This strategy effectively balances global exploration and local exploitation, reducing the number of expensive evaluations and enhancing computational efficiency.

In the following content, this paper presents the problem definition, the proposed KG-HSEA algorithm, experimental analysis and discussion, conclusion and future research directions. This structure systematically addresses the optimization challenges inherent in coal gasification systems.

2. Problem Definition

This section will provide a theoretical explanation of the definition of coal gasification system, construction of surrogate models, and knee point definitions, with a specific focus on their

application in optimizing coal gasification systems to illustrate the practical relevance of these theories.

2.1. Coal gasification system

Taking a plant as an example, it utilizes the multi-component slurry pressurized coal gasification technology. The process flow is shown in Fig. 1. Initially, raw coal is crushed, ground, and mixed with fine slurry, then fed into the coal slurry tank and pumped into the gasifier, where it reacts with pure oxygen to produce raw syngas. The syngas is then washed and cooled in a water scrubber, undergoes a shift process for composition adjustment, and is purified through desulfurization and decarbonization. Finally, the purified syngas is converted into methanol in a synthesis tower under specific conditions, followed by separation and distillation to yield high-purity methanol.

The optimization of operational variables in the coal gasification system becomes an EMOP due to the nonlinear characteristics of the process [26], the complex thermochemical reactions inside the gasifier, and the trade-offs among multiple conflicting objectives.The key variables in the operation process of coal gasification system are reaction temperature(T), gasification agent flow(F_{gas}), reaction pressure(P), air/fuel ratio(A/F_{ratio}) and feed rate(F_{coal}) of raw coal.

A typical multi-objective problem of coal gasification system can be expressed as:

$$\min_{\text{s.t.}x\in\boldsymbol{X}} f(x) = (f_1(x), f_2(x), \cdots, f_M(x)) \tag{1}$$

where, the integer M represents the number of objectives, which is the dimensionality of the solution space, and the set $\boldsymbol{X}$ is the set of feasible decision vectors, and $x = (x_1, x_2, \cdots, x_n)$ is the decision variables of the problem [27].

As one of the objective functions f_1, the energy quality of syngas products is described by heterogeneous integration model, the other objective function f_2 represents the operation stability of the system, expressed in ST and by minimizing the fluctuation range of operation parameters. The specific formula is as follows:

$$\mathrm{ST} = \sum_{p=1}^{P} \left((x_p - x_R)/x_R \right)^2 \tag{2}$$

where x_p represents the real-time value of the pth key operation parameter, x_R is its reference set value, and P is the total number of key operation parameters. The smaller the fluctuation of operation stability, the stronger the stability and the more stable the production process.

In addition, the system energy consumption is taken as the third objective function f_3, which is expressed in SE, the system energy consumption includes fuel cost, oxygen cost and power cost. The specific formula is as follows:

$$\mathrm{SE} = \left(T / \eta_{\text{syngas}}\right) \cdot \left(F_{\text{gas}} + P + A / F_{\text{ratio}}\right) \cdot F_{\text{coal}} \tag{3}$$

where, η_{syngas} represents syngas energy efficiency.

In solving EMOPs of gasification system, a series of non-dominated solutions will ultimately be formed, where each solution in the front is mutually non-dominated. A simple definition of non-dominated solutions is as follows: for a solution set $\boldsymbol{S}$, solution x_1 is called dominant solution x_2, if and only if x_1 is not inferior to x_2 on all objectives and is superior to x_2 on at least one objective. That is to say, for objective j, there are:

$$f_j(x_1) \le f_j(x_2) \tag{4}$$

And there exists an objective k satisfying:

$$f_k(x_1) < f_k(x_2) \tag{5}$$

Among them, the step of sorting the non-dominated solution set is to initialize an empty frontier set, find all non-dominated solutions, and these solutions form the first frontier. Remove the

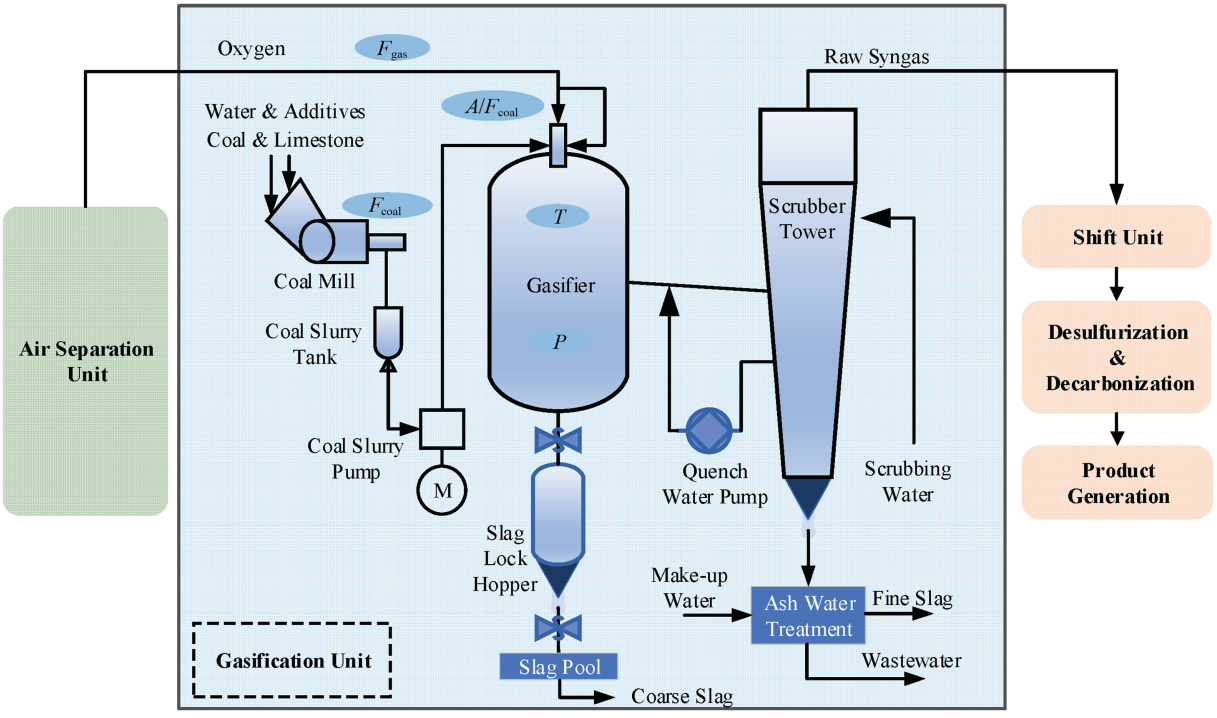

Fig. 1. Process flow diagram of coal gasification system.

solution in the first frontier from the solution set and repeat the above process until all solutions are assigned to a certain frontier.

The non-dominated sorting method (NDSort) divides the solution into multiple frontiers to ensure that the solutions in each frontier are not dominated by other solutions. For each individual P_i in the population, the number of individuals dominated by other individuals in the current population is calculated as nP_i, as well as the set of individuals SP_i dominated by it.

The first frontier F_1 is composed of individuals who are not dominated by any other individual, that is $F_1 = \{P_i \mid nP_i = 0\}$.

Remove from the first frontier and subtract nP_i from the individuals it dominates, then recalculate the number and set of dominants for the remaining individuals in the population. Repeat this process until all individuals are assigned to a certain frontier.

2.2. Composition of heterogeneous surrogate model

In this section, a brief framework of the heterogeneous model will be describe the gasification system. The framework will take five key variables from the coal gasification production process as inputs and uses the energy-quality characteristics of syngas as the output.

(1) Kriging model

This paper selects the Kriging model as part of the heterogeneous surrogate model to approximate each objective function. The Kriging model assumes that the objective function $f(x)$ is a Gaussian process(GP) consisting of a deterministic trend part and a random error part [28], and the basic formula is shown as:

$$f(x) = \mu(x) + \gamma(x), \gamma(x) \sim N\left(0, \sigma^2\right) \tag{6}$$

Among them, μ is a deterministic trend function; $Z(x)$ is GP with zero mean and covariance $\sigma^2 R(\theta)$, σ^2 is the process variance, $R(\theta)$ is the correlation function, and parameter θ controls the shape of the correlation function.

(2) Feedforward neural network(FNN)

During the training process of a FNN model, a non-linear activation function is selected as the sigmoid function between the input layer and the hidden layer [29]. The input is any value, and the output is (0,1). The formula is shown as:

$$g(x) = 1 / (1 + e^{-x}) \tag{7}$$

According to the gradient descent method, calculate the neural weight adjustment amount [30,31]. The weight adjustment amounts between the output layer and hidden layer are shown in Eqs. (8) and (9), respectively.

$$\Delta w_{jk} = -\alpha \delta_k y_j \tag{8}$$

$$\Delta w_{ij} = -\alpha \delta_j y_i \tag{9}$$

where δ_k and δ_j are error terms propagated backward through the network, α is the learning rate, y_i is the input feature, y_j is the output of the hidden neuron.

The architecture of the heterogeneous model is shown in Fig. 2. By combining Kriging's local accuracy and FNN's nonlinear modeling capability through equal fusion of their predictions, the integrated surrogate model achieves enhanced robustness for coal gasification optimization.

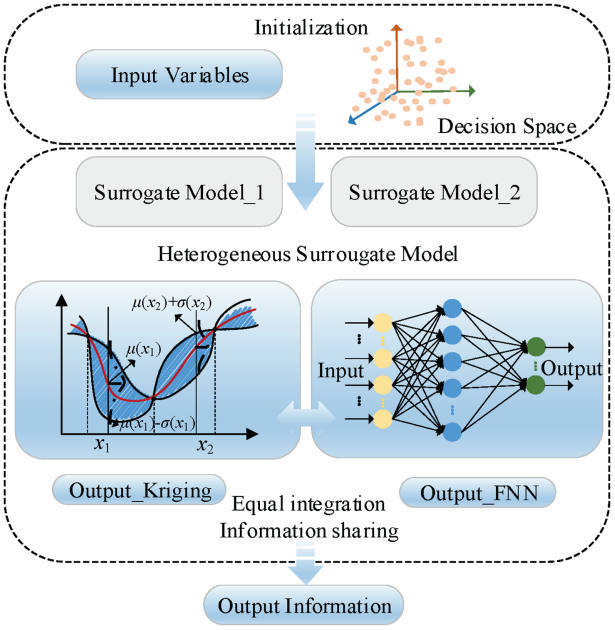

Fig. 2. Heterogeneous surrogate model framework.

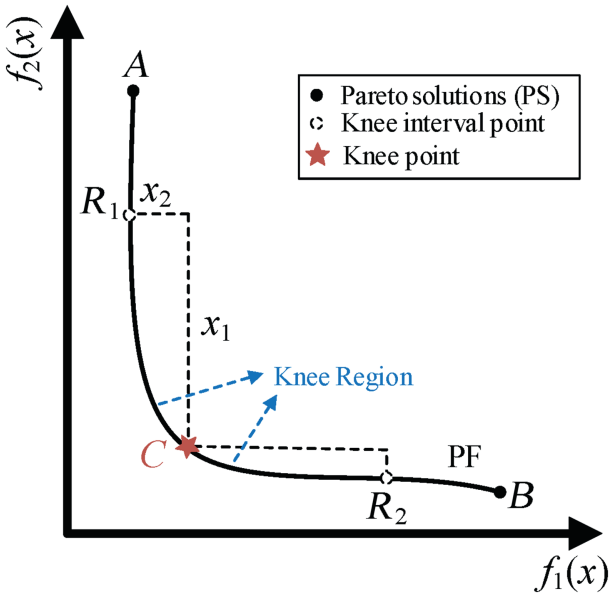

Fig. 3. Schematic diagram of knee points.

2.3. Definition of knee points

Knee Points are solutions on the Pareto front (PF) that exhibit significant inflection points, where any further improvement in one objective results in a pronounced deterioration in at least one other objective, thereby representing an optimal compromise among conflicting targets [29]. As illustrated in Fig. 3, knee point marked C is typically located in the curved region, obtaining a small change x_2 on the objective $f_1(x)$ will cause $f_2(x)$ to make a huge sacrifice x_1. When multiple adjacent solutions on the PF exhibits similar trade-off characteristics, they collectively form a

Knee Region.This region can be quantitatively described through its Knee Interval, defined as the bounded objective-space projection (R_1, R_2) shown in Fig. 3.

Given the complex trade-offs inherent in coal gasification systems, where objectives such as the energy quality of syngas products, system stability, and system energy consumption must be carefully balanced, the identification of knee points becomes particularly valuable. These critical compromise solutions effectively guide the optimization process by focusing the search on regions of the PF that yield the most balanced outcomes for coal gasification operations.

3. KG-HSEA Algorithm

This section introduces the KG-HSEA algorithm, specifically developed for optimizing coal gasification systems under expensive multi-objective constraints. By integrating a heterogeneous surrogate model with a knee point-guided search mechanism, KG-HSEA efficiently balances conflicting objectives while reducing computational costs.

3.1. Heterogeneous model construction

To construct the heterogeneous surrogate model for coal gasification optimization, we employ distinct training strategies for the Kriging and FNN components. For the Kriging model, a Gaussian correlation function is adopted, and model parameters are optimized through cross-validation, enabling robust local approximation in low-dimensional settings.

For the FNN component, we design a network architecture specifically to capture the complex nonlinear patterns in coal gasification data. We utilize the Sigmoid activation function and train the network using relevant data from coal gasification processes, adjusting hyperparameters based on validation data to mitigate overfitting. Finally, the trained model is deployed in practical applications, where it is continuously updated and monitored to ensure adaptation to new input data, thereby maintaining long-term efficiency and accuracy.

3.2. Knee point guidance mechanism

This section will introduce the design process of the knee point-guided mechanism, including the steps of identifying knee points and adding knee points as guidance factors to the overall population evolution process.

To form a guidance mechanism by identifying knee points and selecting solutions with optimal trade-off characteristics, it is necessary to first determine the extremum points, which often represent key positions on the PF. These extremum points are solutions that achieve extreme values on a certain target and reflect important features in the target space. Find the optimal solution set (namely extremum) for each target from the current solution set, use it to fit a hyperplane, and construct a hyperplane based on the maximum solution set to accurately characterize the Pareto frontier morphology. Afterwards, the distance from the extremum point to the hyperplane is calculated, and the knee points on the PF are identified through the neighborhood range to guide the decision-making and optimization process.

(1) Extreme point selection

The KG-HSEA algorithm initiates by employing the NDSort method to classify solutions based on their objective values. From the current Pareto solution set, it finds the maximum point on each target that represents the point at which the objective function reaches its optimal value in the PF, and obtains a candidate set of extreme points for each objective function.

Select for each frontier F_i, and for each objective function f_j, find the solution x_{ij} that achieves the maximum value on that objective:

$$x_{ij} = \arg \max_{x \in F_i} f_j(x) \tag{10}$$

Collect all these maximum values to form the set of maximum points for the current frontier.

According to the sorting results, select the extremum points of each objective function in sequence as the basis for hyperplane calculation, and ensure that the selected extremum points are not repeated, covering the extremum points of each objective function.

(2) Construction of hyperplanes and distance calculation

In a broad sense, a hyperplane is an M-1 dimensional subspace in an M-dimensional space [32]. The linear equation can be described as:

$$a_1x_1 + a_2x_2 + \ldots + a_mx_m = b \tag{11}$$

where, $a_1, a_2, \ldots, a_m$ are the coefficients of the normal vector of the hyperplane, corresponding to the coefficients of the normal vector of the hyperplane in the mth dimension, respectively; $x_1, x_2, \ldots, x_m$ are independent variables, corresponding to the coordinate values on the mth dimension respectively; b is the intercept term of the hyperplane, representing the distance between the hyperplane and the origin.

The EMOPs have M objective functions, each with a maximum point of $F_{i1}, F_{i2}, \ldots, F_{iM}$. It is necessary to find the coefficients $a_1, a_2, \ldots a_m$ so that the hyperplane equation is closest to these maximum points. The hyperplane equation can be expressed as:

$$\sum_{j=1}^{M} a_j \times F_{ij} = 1 \tag{12}$$

Using the least squares method to fit the hyperplane [33], To describe the overall trend of the PF, measure the distance of each solution to the PF, and determine its importance in the target space. Then:

$$\boldsymbol{Fa} = \mathbf{1} \tag{13}$$

Among them, $\boldsymbol{F}$ is a matrix composed of extreme points, and each row represents the target value of an extreme point; $\boldsymbol{a}$ is the coefficient vector of the hyperplane; $\mathbf{1}$ is a vector of all ones.

Determine the coefficient value by minimizing the sum of squared errors as follows:

$$E = \min \|\boldsymbol{Fa} - \mathbf{1}\|^2 \tag{14}$$

Afterwards, calculate the distance from each individual on the PF to the hyperplane. This distance measures the individual's proximity to the PF in the target space and is a key criterion for selecting knee points.

Using geometric methods, calculate the vertical distance from each solution to the hyperplane as a measure of its deviation from the hyperplane. The formula for calculating the distance from each solution to the hyperplane is as follows:

$$d_i = \left| \left(\sum_{j=1}^{M} a_j \times F_{ij} - 1 \right) \right| \Big/ \sqrt{\sum_{j=1}^{M} a_j^2} \tag{15}$$

Among them, d_i is the distance from the ith solution to the hyperplane, F_{ij} represents the value of the ith solution on the jth objective, and a_j is the coefficient of the hyperplane.

(3) Definition and update of neighborhood range

Dynamically adjust the neighborhood search range of each frontier based on the maximum point of the target value in the current frontier, ensuring flexibility and adaptability in selecting knee area points at different positions. Based on the maximum and minimum values of the target values in the current frontier, dynamic adjustment interval $[F_{\min}-\delta, F_{\max}+\delta]$ is set as interval δ [34]. The experiments are conducted using the open-source multi-objective optimization platform PlatEMO, ensuring consistency and reproducibility of the results.

3.3. Experimental configuration

To validate the performance of KG-HSEA in handling high-dimensional, expensive optimization problems, we conduct experiments using standard test functions with varying numbers of objectives. For each test problem, the algorithm is executed independently for 10 runs to ensure statistical reliability. The initial population size is set to 100, and the maximum number of expensive function evaluations (FEs) is restricted to 500, reflecting the computational constraints often encountered in coal gasification system optimization. Performance is assessed using the Inverted Generational Distance (IGD) and spacing metrics, which measure solution quality and distribution uniformity [35]. The operating environment is CPU Intel Core i7-12700K 3.60 GHz, Windows 11 operating system, Matlab 2021b.

3.4. Comparative performance analysis

Tables 1 and 2 respectively provide the average and standard deviation of various multi-objective optimization algorithms, including the algorithm proposed in this paper, under the evaluation of IGD and Spacing metrics. The data highlighted in bold black represents the best results obtained for each evaluation metric. For comprehensive analysis, Table A1 and A2 further provide complete metrics results covering all tested objective dimensions.

To further illustrate algorithm performance, Fig. 4 and Fig. 5 present the population distribution on the WFG6 problem. These visualizations demonstrate how KG-HSEA improves solution spread and convergence, effectively guiding the search toward well-balanced trade-off solutions in coal gasification optimization.

The results in Table 1 indicate that the proposed KG-HSEA algorithm performs well under the Spacing metric across all dimensions of the seven test functions, achieving 11 best results, particularly in DTLZ1, DTLZ2, DTLZ3, and DTLZ6. This demonstrates the algorithm's strong capability in balancing solution diversity and convergence, and this trend is further supported by Appendix A, which shows consistent performance patterns with Table 1, reinforcing KG-HSEA's robustness in diversity maintenance across different benchmark suites. Among the comparison algorithms, ABSAEA achieved 8 best results, highlighting its competitive performance. However, KG-HSEA exhibited slightly weaker results on DTLZ4, DTLZ5, and DTLZ7, trailing behind the corresponding optimal algorithms.

The observed performance limitations on DTLZ4 originate from fundamental challenges in surrogate modeling of discontinuous Pareto fronts. Kriging modeling constraints is one aspect, the stationary Gaussian process assumptions in Kriging lead to substantially increased prediction errors when approximating non-differentiable regions of the PF. This behavior aligns with established theoretical limitations of stationary covariance functions in handling discontinuous surfaces. Besides, the FNN component exhibits reduced accuracy in high-gradient regions due to insufficient sampling density, a direct consequence of the knee-point selection strategy's preferential focus on compromise solutions. These computational characteristics mirror documented challenges in coal gasification system modeling during feedstock transition states [36], where discontinuous parameter variations similarly degrade prediction accuracy. The consistent behavior across synthetic benchmarks and industrial applications suggests this represents a fundamental trade-off in surrogate-assisted optimization of systems with discontinuous dynamics.

While DTLZ2 is relatively easy to converge, it has a high diversity maintenance cost, which can impact solution distribution. In the context of coal gasification system optimization, this reflects the difficulty of maintaining diverse and high-quality solutions when dealing with abrupt changes in reaction conditions, syngas composition, and process stability. The results suggest that KG-HSEA effectively balances these trade-offs, as even in cases where it does not achieve the best numerical results, the performance differences are minor, demonstrating its robustness in addressing highly constrained multi-objective optimization problems.

As shown in Table 2 and Table A2, KG-HSEA demonstrates consistent superiority under the IGD metric across both WFG and DTLZ test set, which outperforms other algorithms under the IGD metric across nine test functions, securing 17 best results on WFG test set. It exhibits particularly strong convergence in WFG3 and WFG6, where maintaining a well-distributed PF is crucial for high-dimensional, computationally expensive problems. This is highly relevant to coal gasification, where optimizing multiple conflicting objectives such as maximizing syngas energy quality while minimizing energy consumption and ensuring system stability, which requires an optimization framework capable of accurately navigating the solution space. The heterogeneous model plays a critical role in this process, as the integration of Kriging and FNN allows for efficient approximation of costly objective functions, significantly reducing computational burden while improving the reliability of predictions.

Despite these advantages, KG-HSEA exhibits relatively weaker performance on specific test cases like DTLZ3, WFG2 and WFG4, where PBRVEA demonstrates comparative advantages. This behavior primarily stems from the knee-region sampling strategy's inherent trade-off between local compromise quality and global exploration capability, particularly when handling problems with complex local optima or high-frequency oscillations. In coal gasification optimization contexts, such scenarios correspond to rare but critical operational transitions including reactor pressure fluctuations, gasification agent flow rate changes, and feedstock composition shifts where specialized handling may be required. It should be emphasized that these limited cases represent boundary conditions rather than typical operational scenarios, as demonstrated by the experimental results across the majority of Tables 1–2

In addition, as shown in Fig. 4, the KG-HSEA algorithm demonstrates a more uniform solution distribution compared to other algorithms, indicating its strong ability to maintain diversity across the PF. This is particularly important in coal gasification system optimization, where a well-distributed solution set enables better adaptability to varying reaction conditions, gasification efficiency, and syngas composition. Furthermore, Fig. 5 illustrates the convergence process of various algorithms on the WFG6 problem, showing that KG-HSEA continuously guides a greater number of solutions toward the PF while preserving uniform

Table 1
Spacing mean and standard deviation of each algorithm on DTLZ test set.

Problem	M	ABSAEA [15]	ADSAPSO [19]	CPSMOEA [22]	PCSAEA [14]	PBRVEA [23]	KG_HSEA
DTLZ1	3	1.5506×10^{1} (5.93)	**3.5968 (3.91)**	6.3865 (3.82)	5.1621 (3.61)	4.0250×10^{1} (2.98×10^{1})	1.3312×10^{1} (6.71)
	4	3.0853×10^{1} (7.62)	2.3011×10^{1} (4.77)	2.2517×10^{1} (2.65)	2.6443×10^{1} (4.79)	3.3476×10^{1} (5.90)	**1.8763×10^{1} (4.80)**
	6	3.4458×10^{1} (3.52)	2.9871×10^{1} (8.57×10^{-1})	2.8537×10^{1} (9.26)	**1.9976×10^{1} (3.99)**	2.7522×10^{1} (2.25)	2.3186×10^{1} (8.66)
	8	3.4728×10^{1} (3.29)	2.5353×10^{1} (7.82)	3.3059×10^{1} (7.19)	2.9795×10^{1} (2.25)	3.1559×10^{1} (4.44)	**1.7009×10^{1} (3.33)**
	10	3.6793×10^{1} (1.32)	3.3821×10^{1} (2.97)	3.8199×10^{1} (4.97)	2.8937×10^{1} (2.31)	**1.7122×10^{1} (1.22×10^{1})**	2.1659×10^{1} (6.74)
DTLZ2	3	7.4765×10^{-2} (2.65×10^{-2})	7.9802×10^{-2} (4.45×10^{-2})	8.6126×10^{-2} (2.37×10^{-2})	1.6443×10^{-1} (3.42×10^{-3})	1.0504×10^{-1} (1.37×10^{-2})	**6.2931×10^{-2} (1.15×10^{-2})**
	4	1.2460×10^{-1} (1.49×10^{-2})	1.9505×10^{-1} (2.00×10^{-2})	2.9845×10^{-1} (2.07×10^{-2})	1.4441×10^{-1} (1.47×10^{-2})	1.3351×10^{-1} (1.02×10^{-2})	**9.3973×10^{-2} (1.02×10^{-2})**
	6	2.2243×10^{-1} (1.36×10^{-2})	2.6860×10^{-1} (2.32×10^{-2})	4.3704×10^{-1} (1.88×10^{-2})	2.5576×10^{-1} (1.37×10^{-2})	**1.9735×10^{-1} (9.45×10^{-3})**	2.6330×10^{-1} (3.88×10^{-3})
	8	2.9380×10^{-1} (3.00×10^{-2})	3.3147×10^{-1} (1.62×10^{-3})	4.8871×10^{-1} (6.54×10^{-2})	3.4008×10^{-1} (3.21×10^{-2})	**2.3868×10^{-1} (1.30×10^{-2})**	3.5105×10^{-1} (3.51×10^{-2})
	10	2.6774 × 10-1 (1.22×10^{-2})	$2.9378 \times$ 10-1 (1.04×10^{-2})	6.4315×10^{-1} (1.26×10^{-1})	2.9983×10^{-1} (1.56×10^{-2})	**2.5208×10^{-1} (3.92×10^{-3})**	4.2620×10^{-1} (2.06×10^{-2})
DTLZ3	3	1.1718×10^{2} (1.10×10^{1})	7.5881×10^{1} (6.72×10^{1})	**4.8647×10^{1} (2.54×10^{1})**	1.4181×10^{2} (3.28×10^{1})	1.2572×10^{2} (1.03×10^{1})	6.6482×10^{1} (6.85)
	4	8.0364×10^{1} (2.20×10^{1})	**3.7759×10^{1} (1.30×10^{1})**	5.3816×10^{1} (9.54)	5.2704×10^{1} (1.17×10^{1})	6.4984×10^{1} (8.64)	4.7750×10^{1} (1.57×10^{1})
	6	8.8989×10^{1} (2.60×10^{1})	9.5726×10^{1} (3.95×10^{1})	9.4736×10^{1} (4.31)	8.1773×10^{1} (2.54×10^{1})	9.5687×10^{1} (1.55×10^{1})	**6.5380×10^{1} (2.42×10^{1})**
	8	5.2447×10^{1} (1.80×10^{1})	3.5274×10^{1} (2.97×10^{1})	8.5798×10^{1} (2.75×10^{1})	3.6087×10^{1} (7.16)	4.5192×10^{1} (1.25×10^{1})	**2.8866×10^{1} (1.10×10^{1})**
	10	1.6368×10^{1} (1.31×10^{1})	**1.0469×10^{1} (1.67×10^{1})**	5.3084×10^{1} (3.62×10^{1})	1.1238×10^{1} (1.01×10^{1})	2.2183×10^{1}(4.68)	2.6458×10^{1} (1.50)
DTLZ4	3	**4.3949×10^{-2} (9.49×10^{-3})**	8.9531×10^{-2} (2.69×10^{-2})	8.4436×10^{-2} (7.01×10^{-2})	8.6636×10^{-2} (1.47×10^{-2})	5.1384×10^{-2} (1.25×10^{-2})	1.4614×10^{-1} (3.16×10^{-1})
	4	1.3947×10^{-1} (2.66×10^{-2})	1.4864×10^{-1} (2.43×10^{-2})	2.2095×10^{-1} (3.91×10^{-2})	**$1.0052 \times$ 10-1 (2.32×10^{-2})**	1.3840×10^{-1} (8.17×10^{-3})	4.6777×10^{-1} (2.70)
	6	2.0090×10^{-1} (3.99×10^{-2})	**1.4070×10^{-1} (1.25×10^{-2})**	2.5955×10^{-1} (1.08×10^{-2})	1.6088×10^{-1} (1.02×10^{-3})	1.9009×10^{-1} (1.51×10^{-2})	8.0784×10^{-1} (5.07)
	8	**$1.1398 \times$ 10-1 (5.22×10^{-3})**	1.8400×10^{-1} (1.16×10^{-1})	1.6378×10^{-1} (1.03×10^{-1})	1.9507×10^{-1} (8.84×10^{-2})	1.3298×10^{-1} (1.57×10^{-2})	8.4464×10^{1} (1.23×10^{1})
	10	1.4948×10^{-1} (1.22×10^{-2})	**9.4144×10^{-2} (1.84×10^{-2})**	8.8639×10^{-1} (7.73×10^{-2})	2.0963×10^{-1} (2.39×10^{-2})	1.8354×10^{-1} (8.24×10^{-3})	2.8598×10^{1} (8.23)
DTLZ5	3	3.5380×10^{-2} (1.43×10^{-2})	1.7629×10^{-2} (9.49×10^{-3})	6.0164×10^{-2} (7.64×10^{-3})	2.1196×10^{-2} (3.22×10^{-3})	3.4923×10^{-3} (1.14×10^{-3})	**1.6772×10^{-3} (3.37×10^{-4})**
	4	**6.7284×10^{-2} (9.00×10^{-3})**	1.0258×10^{-1} (1.47×10^{-2})	1.8863×10^{-1} (2.55×10^{-2})	6.9272×10^{-2} (4.45×10^{-3})	7.8661×10^{-2} (1.19×10^{-2})	7.6328×10^{-2} (8.78×10^{-3})
	6	**9.5991×10^{-2} (1.35×10^{-2})**	1.2853×10^{-1} (4.32×10^{-3})	2.6200×10^{-1} (2.42×10^{-2})	1.0079×10^{-1} (5.66×10^{-3})	1.3413×10^{-1} (1.32×10^{-2})	1.9243×10^{-1} (3.30×10^{-2})
	8	**7.6888×10^{-2} (1.81×10^{-2})**	1.1622×10^{-1} (2.57×10^{-3})	2.6119×10^{-1} (1.17×10^{-2})	9.0555×10^{-2} (1.34×10^{-2})	1.0016×10^{-1} (3.07×10^{-2})	1.5112×10^{-1} (2.14×10^{-2})
	10	5.0115×10^{-2} (3.83×10^{-3})	5.4771×10^{-2} (8.85×10^{-3})	2.1642×10^{-1} (1.79×10^{-2})	6.2011×10^{-2} (1.33×10^{-2})	**3.8503×10^{-2} (1.05×10^{-2})**	8.5601×10^{-2} (1.16×10^{-3})
DTLZ6	3	8.7550×10^{-1} (1.64×10^{-1})	9.3709×10^{-1} (1.04×10^{-1})	8.8983×10^{-1} (9.95×10^{-3})	9.9375×10^{-1} (7.74×10^{-2})	7.3416×10^{-1} (1.97×10^{-2})	**4.9473×10^{-1} (1.16×10^{-1})**
	4	4.6282×10^{-1} (4.43×10^{-3})	7.7322×10^{-1} (8.02×10^{-2})	1.0793 (1.47×10^{-1})	6.3973×10^{-1} (4.78×10^{-2})	4.7700×10^{-1} (2.83×10^{-2})	**4.0996×10^{-1} (6.05×10^{-2})**
	6	6.3201×10^{-1} (3.85×10^{-2})	8.8638×10^{-1} (4.88×10^{-2})	1.2578 (1.34×10^{-1})	7.7279×10^{-1} (4.89×10^{-2})	5.8862×10^{-1} (1.06×10^{-2})	**5.4373×10^{-1} (7.80×10^{-2})**
	8	8.0315×10^{-1} (6.57×10^{-2})	1.0529 (7.04×10^{-2})	1.9478 (5.87×10^{-2})	1.0508 (3.32×10^{-2})	7.5002×10^{-1} (1.42×10^{-1})	**7.2623×10^{-1} (1.00×10^{-1})**
	10	2.2381×10^{-1} (3.17×10^{-2})	3.0126×10^{-1} (3.51×10^{-2})	6.5052×10^{-1} (9.01×10^{-2})	2.4586×10^{-1} (1.76×10^{-2})	**1.4330×10^{-1} (2.14×10^{-2})**	2.6209×10^{-1} (2.94×10^{-2})
DTLZ7	3	**1.1903×10^{-2} (8.67×10^{-3})**	1.0462 (8.18×10^{-2})	1.4892 (5.35×10^{-1})	1.1332 (1.69×10^{-1})	1.4248×10^{-2} (4.93×10^{-3})	1.3706×10^{-2} (2.62×10^{-3})
	4	**8.9928×10^{-2} (2.72×10^{-2})**	1.0876×10^{-1} (7.24×10^{-2})	4.9004×10^{-1} (1.99×10^{-1})	4.5569×10^{-1} (5.77×10^{-1})	2.0787×10^{-1} (2.82×10^{-2})	1.5844×10^{-1} (4.23×10^{-2})
	6	**1.7330×10^{-1} (3.13×10^{-2})**	5.3538×10^{-1} (3.26×10^{-2})	9.9628×10^{-1} (6.85×10^{-2})	5.2130×10^{-1} (1.22×10^{-1})	2.7119×10^{-1} (2.07×10^{-2})	2.8873×10^{-1} (4.21×10^{-2})
	8	**3.1130×10^{-1} (6.07×10^{-2})**	8.4413×10^{-1} (1.65×10^{-1})	1.0557 (3.59×10^{-1})	6.5901×10^{-1} (4.77×10^{-2})	3.7190×10^{-1} (4.48×10^{-2})	4.0274×10^{-1} (1.82×10^{-2})
	10	1.4070 (7.56×10^{-1})	1.1428 (1.51×10^{-2})	2.8033 (4.57×10^{-1})	9.2656×10^{-1} (4.03×10^{-2})	**5.7269×10^{-1} (5.10×10^{-2})**	6.8753×10^{-1} (7.00×10^{-2})

The bold font in each row of the table represents the best performer in the comparative experiment.

Table 2
IGD mean and standard deviation of each algorithm on WFG test set.

Problem	M	ABSAEA	ADSAPSO	CPSMOEA	PCSAEA	PBRVEA	KG_HSEA
WFG1	3	1.6782 (4.62 × 10^{-2})	1.7155 (9.25 × 10^{-2})	2.2801 (1.97 × 10^{-2})	**1.6327 (9.51 × 10^{-2})**	1.6739 (4.02 × 10^{-2})	1.7769 (1.54 × 10^{-1})
	4	1.9154 (1.33 × 10^{-1})	**1.8757 (2.14 × 10^{-2})**	2.4114 (2.15 × 10^{-2})	1.9377 (5.90 × 10^{-2})	2.1347 (2.68 × 10^{-1})	1.9183 (2.95 × 10^{-2})
	6	2.4251 (5.06 × 10^{-2})	2.4536 (7.50 × 10^{-2})	2.7658 (2.40 × 10^{-2})	2.4041 (6.75 × 10^{-2})	**2.2456 (1.85 × 10^{-1})**	2.2860 (1.99 × 10^{-2})
	8	2.8395 (1.41 × 10^{-1})	2.8572 (1.09 × 10^{-1})	3.1303 (2.79 × 10^{-2})	2.9079 (6.55 × 10^{-2})	2.8567 (1.20 × 10^{-1})	**2.7311 (3.86 × 10^{-2})**
	10	3.2763 (1.19 × 10^{-1})	3.3435 (1.31 × 10^{-1})	3.4581 (1.99 × 10^{-2})	3.3051 (2.54 × 10^{-2})	3.2794 (8.31 × 10^{-3})	**2.9448 (1.10 × 10^{-1})**
WFG2	3	5.1314 × 10^{-1} (3.82 × 10^{-2})	6.2653 × 10^{-1} (1.97 × 10^{-1})	6.7820 × 10^{-1} (6.48 × 10^{-2})	4.7508 × 10^{-1} (2.43 × 10^{-2})	**2.1766 × 10^{-1} (1.43 × 10^{-2})**	4.7203 × 10^{-1} (1.26 × 10^{-1})
	4	3.8660 × 10^{-1} (1.36 × 10^{-2})	7.2207 × 10^{-1} (9.53 × 10^{-2})	1.0475 (1.43 × 10^{-1})	6.0630 × 10^{-1} (1.17 × 10^{-2})	**3.3893 × 10^{-1} (2.09 × 10^{-2})**	4.5265 × 10^{-1} (4.86 × 10^{-2})
	6	5.9692 × 10^{-1} (2.54 × 10^{-2})	9.0413 × 10^{-1} (7.47 × 10^{-2})	1.8164 (1.26 × 10^{-1})	8.6959 × 10^{-1} (9.06 × 10^{-2})	**5.1919 × 10^{-1} (2.21 × 10^{-2})**	6.4073 × 10^{-1} (3.48 × 10^{-2})
	8	1.0418 (5.52 × 10^{-2})	1.8044 (1.09)	3.1399 (4.28 × 10^{-1})	1.5481 (3.49 × 10^{-1})	**8.8138 × 10^{-1} (1.21 × 10^{-2})**	1.2912 (2.37 × 10^{-1})
	10	1.6205 (2.23 × 10^{-1})	3.0687 (5.85 × 10^{-1})	3.6112 (3.65 × 10^{-1})	2.8943 (3.79 × 10^{-1})	**1.1430 (9.68 × 10^{-2})**	2.9909 (1.21)
WFG3	3	4.4114 × 10^{-1} (4.59 × 10^{-2})	4.8075 × 10^{-1} (1.14 × 10^{-2})	6.7245 × 10^{-1} (1.55 × 10^{-2})	2.8978 × 10^{-1} (5.10 × 10^{-2})	2.0460 × 10^{-1} (1.08 × 10^{-2})	**1.5351 × 10^{-1} (1.14 × 10^{-2})**
	4	3.1384 × 10^{-1} (8.12 × 10^{-2})	6.4482 × 10^{-1} (3.50 × 10^{-2})	9.0929 × 10^{-1} (1.10 × 10^{-1})	3.6514 × 10^{-1} (1.29 × 10^{-1})	3.5249 × 10^{-1} (1.59 × 10^{-2})	**1.8600 × 10^{-1} (1.24 × 10^{-2})**
	6	4.1836 × 10^{-1} (9.40 × 10^{-3})	6.5754 × 10^{-1} (8.16 × 10^{-2})	1.2451 (2.21 × 10^{-1})	4.1512 × 10^{-1} (1.79 × 10^{-1})	5.7705 × 10^{-1} (3.61 × 10^{-2})	**3.0586 × 10^{-1} (6.60 × 10^{-2})**
	8	8.1733 × 10^{-1} (3.59 × 10^{-2})	1.0683 (4.75 × 10^{-2})	1.7358 (2.45 × 10^{-1})	7.3269 × 10^{-1} (3.89 × 10^{-2})	1.0803 (3.59 × 10^{-1})	**4.9717 × 10^{-1} (3.29 × 10^{-2})**
	10	1.5169 (2.63 × 10^{-2})	1.3914 (8.55 × 10^{-2})	1.9404 (2.24 × 10^{-1})	1.4232 (1.12 × 10^{-1})	1.3227 (4.33 × 10^{-1})	**9.3068 × 10^{-1} (2.81 × 10^{-1})**
WFG4	3	4.5571 × 10^{-1} (2.96 × 10^{-2})	5.9710 × 10^{-1} (4.64 × 10^{-2})	5.9276 × 10^{-1} (1.77 × 10^{-2})	**3.7046 × 10^{-1} (2.40 × 10^{-2})**	3.7416 × 10^{-1} (3.17 × 10^{-2})	4.2499 × 10^{-1} (1.22 × 10^{-2})
	4	6.9384 × 10^{-1} (1.97 × 10^{-2})	9.7710 × 10^{-1} (1.54 × 10^{-1})	1.1646 (2.89 × 10^{-2})	7.5941 × 10^{-1} (1.64 × 10^{-1})	**6.6216 × 10^{-1} (4.72 × 10^{-2})**	8.5223 × 10^{-1} (8.09 × 10^{-2})
	6	1.7398 (3.95 × 10^{-2})	2.2765 (9.81 × 10^{-2})	2.5786 (5.47 × 10^{-2})	1.7320 (7.38 × 10^{-2})	**1.6358 (1.01 × 10^{-1})**	1.7015 (7.99 × 10^{-3})
	8	3.1878 (3.14 × 10^{-1})	4.6459 (6.79 × 10^{-1})	4.3003 (1.36 × 10^{-1})	4.1086 (2.56 × 10^{-1})	**2.7845 (7.65 × 10^{-2})**	3.2874 (2.92 × 10^{-1})
	10	7.7996 (5.87 × 10^{-1})	7.0318 (1.57)	6.0877 (3.38 × 10^{-2})	6.6470 (3.32 × 10^{-1})	**4.8725 (8.33 × 10^{-1})**	5.4030 (2.48 × 10^{-1})
WFG5	3	4.5217 × 10^{-1} (4.16 × 10^{-2})	7.1362 × 10^{-1} (1.39 × 10^{-2})	5.5787 × 10^{-1} (3.71 × 10^{-2})	4.7593 × 10^{-1} (5.70 × 10^{-2})	3.4211 × 10^{-1} (7.77 × 10^{-2})	**2.8747 × 10^{-1} (3.59 × 10^{-2})**
	4	6.5645 × 10^{-1} (2.84 × 10^{-2})	1.0903 (2.13 × 10^{-2})	1.1930 (4.50 × 10^{-2})	7.6604 × 10^{-1} (5.39 × 10^{-2})	8.1174 × 10^{-1} (1.04 × 10^{-1})	**5.7545 × 10^{-1} (4.59 × 10^{-2})**
	6	**1.6468 (5.27 × 10^{-2})**	2.0814 (4.31 × 10^{-2})	2.7548 (7.60 × 10^{-2})	1.7889 (2.05 × 10^{-2})	1.7150 (3.36 × 10^{-2})	1.8871 (3.80 × 10^{-1})
	8	2.9116 (1.90 × 10^{-2})	4.0322 (3.91 × 10^{-1})	4.7108 (8.11 × 10^{-2})	3.3274 (2.86 × 10^{-1})	**2.8687 (7.30 × 10^{-2})**	3.1152 (3.90 × 10^{-2})
	10	5.4816 (5.64 × 10^{-1})	7.3446 (6.57 × 10^{-1})	6.4795 (1.47 × 10^{-1})	5.1358 (5.08 × 10^{-1})	**4.7612 (5.22 × 10^{-1})**	5.3337 (2.23 × 10^{-1})
WFG6	3	6.5399 × 10^{-1} (2.31 × 10^{-2})	8.2462 × 10^{-1} (5.64 × 10^{-2})	8.2565 × 10^{-1} (5.58 × 10^{-2})	6.2972 × 10^{-1} (1.29 × 10^{-2})	4.8165 × 10^{-1} (1.43 × 10^{-1})	**4.3646 × 10^{-1} (4.54 × 10^{-2})**
	4	1.0975 (4.06 × 10^{-2})	1.1403 (1.26 × 10^{-1})	1.3836 (4.08 × 10^{-2})	8.9022 × 10^{-1} (6.35 × 10^{-2})	8.3601 × 10^{-1} (2.01 × 10^{-2})	**7.3991 × 10^{-1} (4.81 × 10^{-2})**
	6	2.2397 (1.58 × 10^{-1})	2.0520 (9.09 × 10^{-2})	2.7742 (5.04 × 10^{-2})	1.9092 (8.07 × 10^{-2})	1.8290 (5.47 × 10^{-2})	**1.7222 (5.28 × 10^{-2})**
	8	3.6817 (9.81 × 10^{-2})	4.2158 (2.63 × 10^{-1})	4.5499 (1.41 × 10^{-1})	3.8957 (3.87 × 10^{-1})	3.2436 (8.13 × 10^{-2})	**3.1069 (4.95 × 10^{-2})**
	10	6.4010 (3.17 × 10^{-1})	6.8507 (3.08 × 10^{-1})	7.4235 (4.64 × 10^{-1})	6.1259 (2.15 × 10^{-1})	5.1748 (1.07 × 10^{-1})	**4.8515 (2.23 × 10^{-1})**
WFG7	3	5.1993 × 10^{-1} (6.65 × 10^{-2})	5.9750 × 10^{-1} (3.52 × 10^{-3})	6.4665 × 10^{-1} (6.58 × 10^{-3})	**4.7680 × 10^{-1} (3.66 × 10^{-2})**	5.4770 × 10^{-1} (3.67 × 10^{-2})	5.4976 × 10^{-1} (2.81 × 10-2)
	4	7.8962 × 10^{-1} (3.99 × 10^{-2})	9.5598 × 10^{-1} (3.28 × 10^{-2})	1.2597 (4.08 × 10^{-2})	7.7286 × 10^{-1} (5.16 × 10^{-2})	**7.3984 × 10^{-1} (3.80 × 10^{-2})**	8.4773 × 10^{-1} (1.32 × 10^{-2})
	6	1.9973 (1.04 × 10^{-1})	2.3147 (2.27 × 10^{-1})	2.6622 (4.99 × 10^{-2})	1.8851 (1.45 × 10^{-1})	1.6753 (3.60 × 10^{-2})	**1.6738 (5.82 × 10^{-2})**
	8	3.7503 (3.94 × 10^{-1})	4.6336 (1.51 × 10^{-1})	5.1154 (1.26 × 10^{-1})	3.9173 (3.21 × 10^{-1})	**2.8093 (1.97 × 10^{-2})**	3.0180 (5.18 × 10^{-2})
	10	6.1142 (2.97 × 10^{-1})	7.0587 (3.91 × 10^{-1})	7.9186 (2.46 × 10^{-1})	7.1296 (8.45 × 10^{-1})	**4.6223 (6.85 × 10^{-2})**	5.2453 (1.25)
WFG8	3	5.3559 × 10^{-1} (7.70 × 10^{-2})	7.3392 × 10^{-1} (8.41 × 10^{-2})	8.3311 × 10^{-1} (5.83 × 10^{-2})	5.9713 × 10^{-1} (2.38 × 10^{-2})	**4.1203 × 10^{-1} (2.38 × 10^{-2})**	4.1443 × 10^{-1} (2.85 × 10^{-2})
	4	1.1770 (6.77 × 10^{-2})	1.2935 (4.17 × 10^{-2})	1.4946 (3.08 × 10^{-2})	1.1047 (2.22 × 10^{-2})	**8.6103 × 10^{-1} (3.78 × 10^{-2})**	8.7255 × 10^{-1} (2.22 × 10^{-2})
	6	2.6060 (1.22 × 10^{-1})	2.5651 (9.19 × 10^{-2})	2.9252 (5.16 × 10^{-2})	2.5681 (1.05 × 10^{-1})	**2.0377 (6.10 × 10^{-2})**	2.0562 (4.04 × 10^{-2})
	8	4.3976 (8.91 × 10^{-2})	4.5064 (5.95 × 10^{-1})	4.7456 (1.10 × 10^{-1})	4.5588 (5.25 × 10^{-1})	**3.2408 (9.62 × 10^{-2})**	3.6120 (3.40 × 10^{-2})
	10	7.3782 (4.73 × 10^{-1})	6.8963 (7.84 × 10^{-1})	7.1464 (1.28 × 10^{-1})	7.1186 (4.91 × 10^{-1})	5.6471 (8.28 × 10^{-1})	**5.2597 (1.72 × 10^{-1})**
WFG9	3	4.8679 × 10^{-1} (1.14 × 10^{-1})	6.4791 × 10^{-1} (8.42 × 10^{-2})	5.9353 × 10^{-1} (7.50 × 10^{-2})	**4.3347 × 10^{-1} (4.81 × 10^{-2})**	5.8007 × 10^{-1} (7.81 × 10^{-2})	5.4358 × 10^{-1} (5.79 × 10^{-2})
	4	**7.7901 × 10^{-1} (8.52 × 10^{-2})**	1.1077 (5.95 × 10^{-2})	1.4220 (5.89 × 10^{-2})	8.9523 × 10^{-1} (5.13 × 10^{-2})	8.4118 × 10^{-1} (7.28 × 10^{-2})	1.0154 (1.98 × 10^{-1})
	6	**1.7789 (1.60 × 10^{-1})**	2.0960 (1.44 × 10^{-1})	2.9690 (1.28 × 10^{-1})	1.8059 (8.85 × 10^{-2})	1.9496 (1.90 × 10^{-1})	2.1748 (4.47 × 10^{-2})
	8	**3.2311 (1.78 × 10^{-1})**	4.1519 (2.35 × 10^{-1})	4.9748 (1.46 × 10^{-1})	3.7871 (1.76 × 10^{-1})	3.3291 (2.72 × 10^{-1})	3.8257 (3.64 × 10^{-1})
	10	5.9838 (5.70 × 10^{-1})	7.4975 (4.40 × 10^{-1})	7.6010 (9.42 × 10^{-2})	6.7023 (2.52 × 10^{-1})	7.2614 (6.43 × 10^{-1})	**5.7064 (5.02 × 10^{-1})**

The bold font in each row of the table represents the best performer in the comparative experiment.

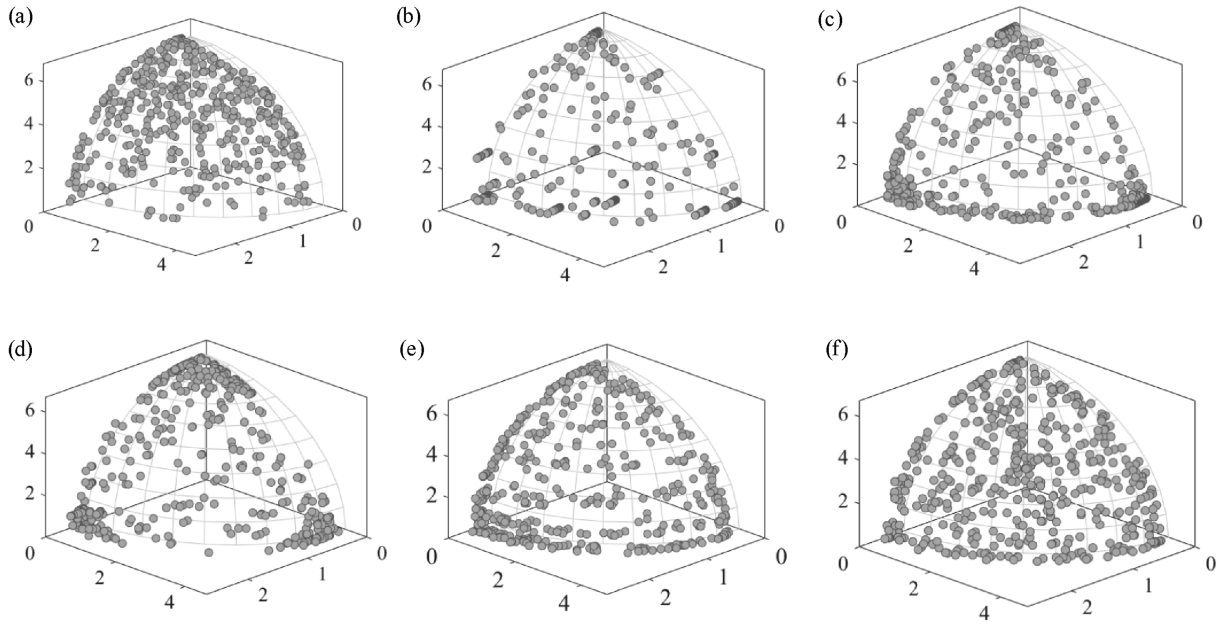

Fig. 4. The population distribution of various algorithms on the WFG6 problem. (a) Distribution presented by ABSAEA, (b) Distribution presented by ADSAPSO, (c) Distribution presented by CPSMOEA, (d) Distribution presented by PCSAEA, (e) Distribution presented by PBRVEA, (f) Distribution presented by KG-HSEA.

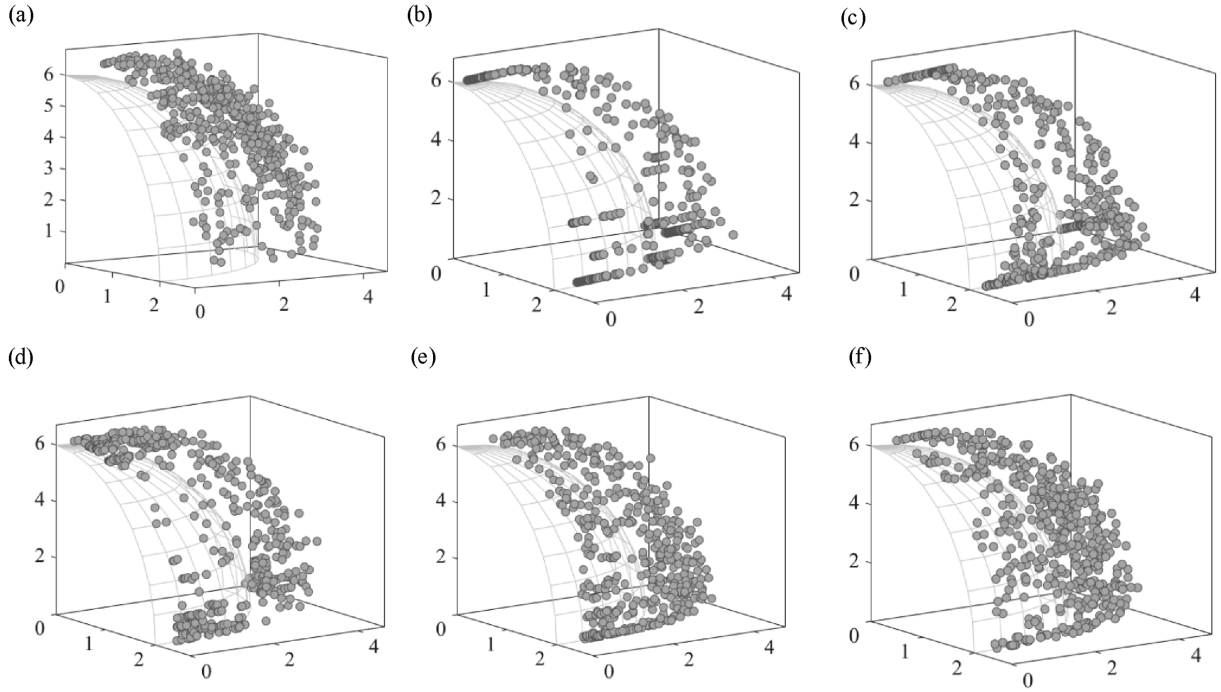

Fig. 5. The convergence of various algorithms on the WFG6 problem. (a) Convergence presented by ABSAEA, (b) Convergence presented by ADSAPSO, (c) Convergence presented by CPSMOEA, (d) Convergence presented by PCSAEA, (e) Convergence presented by PBRVEA, (f) Convergence presented by KG-HSEA.

distribution. This highlights the effectiveness of the knee point-guided mechanism, which helps the algorithm identify critical trade-off solutions and achieve a more balanced optimization across conflicting objectives.

3.5. Discussion of the proposed method

Through multiple metrics, we evaluated the effectiveness of KG-HSEA on EMOPs related to coal gasification. Notably, the proposed algorithm achieved the best performance on 23 of 32 benchmark problems, derived from 16 test functions evaluated under two metrics, with a 71.9% superiority rate, significantly outperforming the competitors. Although the algorithm exhibited slightly weaker performance in a few test cases, this behavior, from a computational learning perspective, reflects the intrinsic difficulty faced by surrogate-assisted evolutionary algorithms in maintaining consistent approximation quality across both smooth and non-smooth regions of the objective space, as

highlighted in theoretical analyses of heterogeneous surrogate frameworks [37].

Overall, KG-HSEA demonstrated strong competitiveness without evident drawbacks compared to other methods. Its ability to efficiently approximate expensive functions *via* a heterogeneous surrogate model ensures its computational feasibility for complex coal gasification optimization tasks. To further improve robustness in discontinuous or irregular regions, future research could investigate adaptive kernel selection or hybrid sampling mechanisms, aiming to enhance generalization without compromising convergence guarantees. Advances in heterogeneous surrogate modeling may also improve the adaptability and performance of KG-HSEA on high-dimensional, computationally expensive multi-objective problems.

4. Conclusions

In our research, we proposed a process-oriented design that addresses the multi-objective optimization challenges in coal gasification systems. We developed the KG-HSEA, a heterogeneous surrogate-assisted evolutionary algorithm that incorporates a knee point-guided mechanism to meet the industrial requirements of balancing syngas energy quality, system stability, and energy consumption. The integration of Kriging and FNN allows for a more accurate approximation of the complex solution space, while the adaptive dual-archive management strategy ensures robust convergence and diversity in the optimization process. Experimental results confirm that the proposed approach produces a well-balanced set of operational parameters, thereby enhancing overall system performance and providing valuable guidance for practical coal gasification optimization.

Although the methodology demonstrates promise in terms of accuracy, efficiency, and generalization, challenges remain, particularly in updating models to adapt to dynamically changing process conditions. Future work will focus on further refining heterogeneous model integration and population evolution strategies to reduce computation time and improve adaptability, ultimately contributing to more effective process optimization in complex industrial environments.

CRediT authorship contribution statement

Wenlu Li: Writing – review & editing, Writing – original draft, Visualization, Validation, Supervision, Software, Resources, Project administration, Methodology, Formal analysis, Data curation, Conceptualization. **Nan Guo:** Validation, Supervision, Methodology, Funding acquisition, Conceptualization. **Tiewei Shang:** Visualization, Validation, Supervision, Software, Formal analysis. **Yueyang Sun:** Writing – review & editing, Validation, Supervision, Software, Methodology, Conceptualization. **Dapeng Li:** Writing – review & editing, Visualization, Validation, Supervision, Formal analysis. **Xiaolong Gao:** Validation, Supervision, Project administration. **Wei Xiong:** Validation, Supervision, Resources, Investigation, Formal analysis. **Junfei Qiao:** Validation, Supervision, Project administration, Methodology, Investigation, Funding acquisition, Formal analysis, Data curation, Conceptualization.

Declaration of Competing Interest

The authors declare that they have no known competing financial interests or personal relationships that could have appeared to influence the work reported in this paper.

Acknowledgements

This work was supported by Scientific and Technological Innovation 2030 - "New Generation Artificial Intelligence" Major Project (2021ZD0112301), Science Fund for Creative Research Groups of the National Natural Science (62021003), the National Natural Science Foundation of China (62303027), The open project of China Food Flavor and Nutrition Health Innovation Center (CFC2023B-021).

References

[1] M. Wiatowski, W. Basa, M. Pankiewicz-Sperka, M. Szyja, H.R. Thomas, R. Zagorscak, S. Sadasivam, S. Masum, T. Kempka, C. Otto, K. Kapusta, Experimental study on tar formation during underground coal gasification: Effect of coal rank and gasification pressure on tar yield and chemical composition, *Fuel* 357 (2024) 130034.
[2] R.Q. Mu, M. Liu, J.J. Yan, Advanced exergy analysis on supercritical water gasification of coal compared with conventional O_2-H_2O and chemical looping coal gasification, *Fuel Process. Technol.* 245 (2023) 107742.
[3] Z. Shen, Z.Y. Huang, High-efficiency and pollution-controlling *in-situ* gasification chemical looping combustion system by using CO_2 instead of steam as gasification agent, *Chin. J. Chem. Eng.* 26 (11) (2018) 2368–2376.
[4] Y. Cui, J. Liang, Z.Q. Wang, X.C. Zhang, C.Z. Fan, D.Y. Liang, X. Wang, Forward and reverse combustion gasification of coal with production of high-quality syngas in a simulated pilot system for *in situ* gasification, *Appl. Energy* 131 (2014) 9–19.
[5] T.H. Duan, C.P. Lu, S. Xiong, Z.B. Fu, B. Zhang, Evaluation method of the energy conversion efficiency of coal gasification and related applications, *Int. J. Energy Res.* 40 (2) (2016) 168–180.
[6] X.Y. Yao, W.H. Li, X.G. Pan, R. Wang, Multimodal multi-objective evolutionary algorithm for multiple path planning, *Comput. Ind. Eng.* 169 (2022) 108145.
[7] F. Xie, M. An, P. Li, X.D. Hu, H.C. Bai, Q.J. Guo, Simulation study on the gasification process of Ningdong coal with iron-based oxygen carrier, *Chin. J. Chem. Eng.* 29 (2021) 326–334.
[8] L. Huang, L. Qi, H.N. Wang, J.L. Zhang, X.Q. Jia, Optimal design of heat exchanger header for coal gasification in supercritical water through CFD simulations, *Chin. J. Chem. Eng.* 25 (8) (2017) 1101–1108.
[9] S.S. Ye, Q. Tang, Y.D. Wang, W.Y. Fei, Structural optimization of a settler *via* CFD simulation in a mixer-settler, *Chin. J. Chem. Eng.* 28 (4) (2020) 995–1015.
[10] J.P. Luo, Y.F. Dong, Q.Q. Liu, Z.X. Zhu, W.M. Cao, K.C. Tan, Y.C. Jin, A new multitask joint learning framework for expensive multi-objective optimization problems, *IEEE Trans. Emerg. Top. Comput. Intell.* 8 (2) (2024) 1894–1909.
[11] B.D. Li, Y.T. Yang, D.C. Liu, Y. Zhang, A.M. Zhou, X. Yao, Accelerating surrogate assisted evolutionary algorithms for expensive multi-objective optimization *via* explainable machine learning, *Swarm Evol. Comput.* 88 (2024) 101610.
[12] S. Kuhnt, D.M. Steinberg, Design and analysis of computer experiments, *Asta Adv. Stat. Anal.* 94 (4) (2010) 307–309.
[13] L.Q. Pan, C. He, Y. Tian, H.D. Wang, X.Y. Zhang, Y.C. Jin, A classification-based surrogate-assisted evolutionary algorithm for expensive many-objective optimization, *IEEE Trans. Evol. Comput.* 23 (1) (2019) 74–88.
[14] Y. Tian, J.X. Hu, C. He, H.P. Ma, L.M. Zhang, X.Y. Zhang, A pairwise comparison based surrogate-assisted evolutionary algorithm for expensive multi-objective optimization, *Swarm Evol. Comput.* 80 (2023) 101323.
[15] X.L. Wang, Y.C. Jin, S. Schmitt, M. Olhofer, An adaptive Bayesian approach to surrogate-assisted evolutionary multi-objective optimization, *Inf. Sci.* 519 (2020) 317–331.
[16] N.V. Queipo, R.T. Haftka, W. Shyy, T. Goel, R. Vaidyanathan, P. Kevin Tucker, Surrogate-based analysis and optimization, *Prog. Aerosp. Sci.* 41 (1) (2005) 1–28.
[17] C.L. Hua, Y.C. Cui, F. Wu, R.D. Zhang, Enhanced process monitoring for industrial coking furnace using a dual-channel pooling and homologous bilinear model-based convolutional neural network, *Can. J. Chem. Eng.* 102 (8) (2024) 2857–2875.
[18] E. Lughofer, R. Pollak, C. Feilmayr, M. Schatzl, S. Saminger-Platz, Prediction and explanation models for hot metal temperature, silicon concentration, and cooling capacity in ironmaking blast furnaces, *Steel Res. Int.* 92 (9) (2021) 2100078.
[19] J.Q. Lin, C. He, R. Cheng, Adaptive dropout for high-dimensional expensive multiobjective optimization, *Complex Intell. Syst.* 8 (1) (2022) 271–285.
[20] F. Li, L. Gao, W.M. Shen, Surrogate-assisted multi-objective evolutionary optimization with Pareto front model-based local search method, *IEEE Trans. Cybern.* 54 (1) (2024) 173–186.
[21] R. Snaiki, A. Jamali, A. Rahem, M. Shabani, B.L. Barjenbruch, A metaheuristic-optimization-based neural network for icing prediction on transmission lines, *Cold Reg. Sci. Technol.* 224 (2024) 104249.
[22] J.Y. Zhang, A.M. Zhou, G.X. Zhang, A classification and Pareto domination based multiobjective evolutionary algorithm, IEEE, Sendai, Japan, 2015.

[23] Z.S. Song, H.D. Wang, H.B. Xu, A framework for expensive many-objective optimization with Pareto-based bi-indicator infill sampling criterion, *Memet. Comput.* 14 (2) (2022) 179−191.
[24] X.Y. Zhang, Y. Tian, Y.C. Jin, A knee point-driven evolutionary algorithm for many-objective optimization, *IEEE Trans. Evol. Comput.* 19 (6) (2014) 761−776.
[25] J. Zou, Q.Y. Li, S.X. Yang, H. Bai, J.H. Zheng, A prediction strategy based on center points and knee points for evolutionary dynamic multi-objective optimization, *Appl. Soft Comput.* 61 (2017) 806−818.
[26] A. Konak, D.W. Coit, A.E. Smith, Multi-objective optimization using genetic algorithms: a tutorial, *Reliab. Eng. Syst. Saf.* 91 (9) (2006) 992−1007.
[27] C.L. Park, B.G. Kim, The optimization of low-rank coal grinding for transport coal gasification by robust design, *Fuel* 95 (2012) 282−286.
[28] J. Sacks, W.J. Welch, T.J. Mitchell, H.P. Wynn, Design and analysis of computer experiments, *Statist. Sci.* 4 (4) (1989) 433−435.
[29] H. Jaeger, M. Lukosevicius, D. Popovici, U. Siewert, Optimization and applications of echo state networks with leaky-integrator neurons, *Neural Netw.* 20 (3) (2007) 335−352.
[30] L. Rachmawati, D. Srinivasan, Multiobjective evolutionary algorithm with controllable focus on the knees of the Pareto front, *IEEE Trans. Evol. Comput.* 13 (4) (2009) 810−824.
[31] J.F. Qiu, M.H. Liu, L. Zhang, W. Li, F. Cheng, A multi-level knee point based multi-objective evolutionary algorithm for AUC maximization, *Memet. Comput.* 11 (3) (2019) 285−296.
[32] H.K. Chen, Y. Tian, W. Pedrycz, G.H. Wu, R. Wang, L. Wang, Hyperplane assisted evolutionary algorithm for many-objective optimization problems, *IEEE Trans. Cybern.* 50 (7) (2019) 3367−3380.
[33] R.V. Lenth, Least-squares means: The *R*Packagelsmeans, *J. Stat. Soft.* 69 (1) (2016) 1−33.
[34] K. Deb, L. Thiele, M. Laumanns, E. Zitzler, Scalable multi-objective optimization test problems. Proceedings of the 2002 Congress on Evolutionary Computation, Honolulu, HI, USA, IEEE, 2002, pp. 825−830.
[35] C.A. Coello Coello, M. Reyes-Sierra, Multi-objective particle swarm optimizers: a survey of the state-of-the-art, *Int. J. Comput. Intell. Res.* 2 (3) (2006) 287−308.
[36] X.D. Kong, W.M. Zhong, W.L. Du, F. Qian, Compartment modeling of coal gasification in an entrained flow gasifier: a study on the influence of operating conditions, *Energy Convers. Manag.* 82 (2014) 202−211.
[37] X.B. Shang, Z. Zhang, H. Fang, B. Li, Y.H. Li, Ensemble learning of multi-kernel Kriging surrogate models using regional discrepancy and space-filling criteria-based hybrid sampling method, *Adv. Eng. Inform.* 58 (2023) 102186.

Appendix

Table A1
Spacing mean and standard deviation of each algorithm on WFG test set

Problem	M	ABSAEA	ADSAPSO	CPSMOEA	PCSAEA	PBRVEA	KG_HSEA
WFG1	3	1.3734×10^{-1} (1.62×10^{-2})	1.8038×10^{-1} (3.67×10^{-2})	2.2870×10^{-1} (1.45×10^{-2})	1.4490×10^{-1} (2.90×10^{-2})	**1.0638×10^{-1} (4.04×10^{-2})**	1.7633×10^{-1} (6.68×10^{-2})
	4	5.3113×10^{-1} (3.17×10^{-1})	**2.3192×10^{-1} (6.45×10^{-2})**	1.3560 (9.36×10^{-2})	6.1067×10^{-1} (1.09×10^{-1})	3.4223×10^{-1} (4.00×10^{-2})	4.1956×10^{-1} (4.57×10^{-3})
	6	5.1002×10^{-1} (5.59×10^{-2})	**1.4629×10^{-1} (7.74×10^{-2})**	1.8833 (8.51×10^{-2})	8.3974×10^{-1} (5.24×10^{-2})	2.4993×10^{-1} (2.35×10^{-1})	5.4235×10^{-1} (4.66×10^{-2})
	8	3.8606×10^{-1} (2.99×10^{-1})	2.9514×10^{-1} (9.42×10^{-2})	2.3848 (1.99×10^{-2})	1.1725 (1.01×10^{-1})	**1.3401×10^{-1} (8.91×10^{-2})**	8.2869 $\times 10^{-1}$ (1.86×10^{-1})
	10	4.0765×10^{-1} (2.84×10^{-1})	4.6654×10^{-1} (3.57×10^{-1})	2.7084 (2.35×10^{-1})	1.0221 (6.60×10^{-1})	4.3017×10^{-1} (4.39×10^{-1})	**1.5026×10^{-1} (4.92×10^{-2})**
WFG2	3	6.7140×10^{-2} (6.46×10^{-3})	1.1314×10^{-1} (5.22×10^{-2})	1.0271×10^{-1} (1.10×10^{-2})	5.0754×10^{-2} (1.32×10^{-2})	**1.3466×10^{-2} (1.92×10^{-3})**	4.6128×10^{-2} (1.63×10^{-2})
	4	2.4085×10^{-1} (4.64×10^{-2})	4.6948×10^{-1} (1.05×10^{-1})	5.1300×10^{-1} (1.08×10^{-1})	3.3183×10^{-1} (1.01×10^{-1})	2.6385×10^{-1} (3.29×10^{-2})	**2.3113×10^{-1} (2.51×10^{-2})**
	6	**3.8052×10^{-1} (3.78×10^{-2})**	5.7270×10^{-1} (8.21×10^{-2})	$1.3136 (1.91 \times 10^{-1})$	5.7297×10^{-1} (4.93×10^{-2})	5.9441×10^{-1} (4.76×10^{-2})	5.9188×10^{-1} (4.66×10^{-2})
	8	**6.6732×10^{-1} (1.78×10^{-1})**	7.5878×10^{-1} (4.73×10^{-2})	$1.6355 (1.82 \times 10^{-1})$	9.7089×10^{-1} (8.11×10^{-2})	6.8361×10^{-1} (3.03×10^{-2})	6.7630×10^{-1} (5.84×10^{-2})
	10	$1.6555 (2.90 \times 10^{-1})$	$1.6657 (4.35 \times 10^{-1})$	$1.9589 (2.25 \times 10^{-1})$	$1.0516 (6.08 \times 10^{-2})$	**8.9443×10^{-1} (2.31×10^{-1})**	9.2596×10^{-1} (1.05×10^{-1})
WFG3	3	7.7919×10^{-2} (4.73×10^{-3})	8.6770×10^{-2} (5.11×10^{-3})	1.6342×10^{-1} (6.61×10^{-3})	5.4281×10^{-2} (2.45×10^{-3})	**3.5835×10^{-2} (3.18×10^{-3})**	3.6647×10^{-2} (6.32×10^{-3})
	4	2.2222×10^{-1} (1.62×10^{-3})	3.0667×10^{-1} (3.13×10^{-2})	4.6160×10^{-1} (6.49×10^{-2})	2.0693×10^{-1} (3.25×10^{-2})	**1.6947×10^{-1} (1.39×10^{-2})**	1.8397×10^{-1} (7.72×10^{-3})
	6	5.5191×10^{-1} (4.73×10^{-2})	5.4320×10^{-1} (4.35×10^{-2})	$1.0196 (1.07 \times 10^{-1})$	**4.5998×10^{-1} (9.60×10^{-3})**	4.6051×10^{-1} (1.67×10^{-2})	4.6342×10^{-1} (1.66×10^{-2})
	8	8.1508×10^{-1} (3.71×10^{-3})	7.1596×10^{-1} (2.77×10^{-2})	$1.5375 (1.31 \times 10^{-1})$	7.1804×10^{-1} (1.84×10^{-2})	7.5392×10^{-1} (7.43×10^{-2})	**7.0920×10^{-1} (2.13×10^{-2})**
	10	$1.0182 (5.06 \times 10^{-2})$	**8.7887×10^{-1} (1.34×10^{-2})**	$1.8158 (3.24 \times 10^{-1})$	9.6014×10^{-1} (1.69×10^{-2})	8.7984×10^{-1} (1.29×10^{-1})	9.7052×10^{-1} (8.65×10^{-2})
WFG4	3	3.6754×10^{-2} (3.06×10^{-3})	6.5479×10^{-2} (1.38×10^{-2})	6.2514×10^{-2} (1.28×10^{-3})	2.6890×10^{-2} (1.80×10^{-3})	**2.6405×10^{-2} (3.19×10^{-3})**	3.4105×10^{-2} (3.98×10^{-3})
	4	4.1445×10^{-1} (1.19×10^{-2})	5.8220×10^{-1} (3.69×10^{-2})	8.5944×10^{-1} (1.02×10^{-1})	**3.8937×10^{-1} (1.65×10^{-3})**	3.9207×10^{-1} (1.89×10^{-2})	4.6218×10^{-1} (4.83×10^{-2})
	6	$1.1325 (7.13 \times 10^{-2})$	$1.0854 (6.08 \times 10^{-2})$	$1.7971 (1.24 \times 10^{-1})$	**$1.0197 (2.30 \times 10^{-2})$**	$1.1141 (4.69 \times 10^{-2})$	$1.0833 (3.77 \times 10^{-2})$
	8	$1.9022 (1.42 \times 10^{-1})$	**$1.5118 (2.04 \times 10^{-1})$**	$2.9744 (3.53 \times 10^{-1})$	$1.6557 (2.73 \times 10^{-1})$	$1.9291 (3.49 \times 10^{-2})$	$1.8822 (4.98 \times 10^{-2})$
	10	$2.5379 (2.70 \times 10^{-1})$	$2.2281 (2.58 \times 10^{-1})$	$4.5006 (2.66 \times 10^{-1})$	**$2.1122 (1.40 \times 10^{-1})$**	$2.5776 (3.40 \times 10^{-1})$	$2.6307 (2.27 \times 10^{-1})$
WFG5	3	4.4381×10^{-2} (6.31×10^{-3})	1.0464×10^{-1} (4.87×10^{-3})	6.3308×10^{-2} (3.89×10^{-3})	4.3254×10^{-2} (4.38×10^{-3})	2.1825×10^{-2} (9.72×10^{-3})	**1.3244×10^{-2} (2.55×10^{-3})**
	4	4.6705×10^{-1} (4.53×10^{-3})	6.3814×10^{-1} (7.23×10^{-3})	5.8438×10^{-1} (1.43×10^{-1})	4.3158×10^{-1} (2.88×10^{-2})	4.8579×10^{-1} (1.98×10^{-2})	**4.0388×10^{-1} (5.57×10^{-3})**
	6	**9.9169×10^{-1} (2.85×10^{-2})**	$1.2452 (1.10 \times 10^{-1})$	$1.5165 (9.75 \times 10^{-2})$	$1.0459 (1.86 \times 10^{-2})$	$1.1361 (4.36 \times 10^{-2})$	$1.1059 (1.86 \times 10^{-2})$
	8	**$1.7589 (4.62 \times 10^{-2})$**	$2.0826 (1.72 \times 10^{-1})$	$2.3615 (9.76 \times 10^{-2})$	$1.8841 (4.00 \times 10^{-2})$	$1.8859 (4.36 \times 10^{-2})$	$1.8884 (5.57 \times 10^{-2})$
	10	$2.9425 (2.29 \times 10^{-1})$	$3.2293 (2.58 \times 10^{-1})$	$2.9319 (4.37 \times 10^{-1})$	$2.8246 (1.12 \times 10^{-1})$	**$2.7626 (1.61 \times 10^{-1})$**	$2.9150 (2.71 \times 10^{-1})$
WFG6	3	5.9071×10^{-2} (1.70×10^{-3})	1.2706×10^{-1} (5.42×10^{-3})	1.2203×10^{-1} (4.35×10^{-3})	6.6854×10^{-2} (4.58×10^{-3})	4.3739×10^{-2} (2.07×10^{-2})	**3.2009×10^{-2} (5.79×10^{-3})**
	4	5.0051×10^{-1} (2.24×10^{-2})	6.2680×10^{-1} (1.39×10^{-1})	7.9200×10^{-1} (1.05×10^{-1})	4.8702×10^{-1} (1.43×10^{-2})	4.3603×10^{-1} (2.60×10^{-2})	**3.8840×10^{-1} (1.49×10^{-2})**
	6	$1.2554 (3.86 \times 10^{-2})$	$1.3545 (1.77 \times 10^{-2})$	$1.6429 (1.01 \times 10^{-1})$	$1.1464 (1.05 \times 10^{-1})$	$1.1676 (6.98 \times 10^{-2})$	**$1.0485 (5.76 \times 10^{-2})$**
	8	$2.1649 (1.08 \times 10^{-1})$	$2.0323 (2.18 \times 10^{-1})$	**$1.9205 (8.90 \times 10^{-2})$**	$1.9595 (6.91 \times 10^{-2})$	$2.1968 (1.20 \times 10^{-1})$	$2.6315 (3.89 \times 10^{-1})$
	10	$2.8810 (1.85 \times 10^{-1})$	$3.1301 (1.32 \times 10^{-1})$	$6.7089 (4.70 \times 10^{-1})$	$2.8778 (9.91 \times 10^{-2})$	**$2.7899 (1.04 \times 10^{-1})$**	$3.0994 (2.69 \times 10^{-1})$
WFG7	3	4.7856×10^{-2} (1.21×10^{-2})	4.1449×10^{-2} (7.73×10^{-3})	8.3393×10^{-2} (4.44×10^{-3})	**3.8907×10^{-2} (5.01×10^{-3})**	4.8020×10^{-2} (3.19×10^{-3})	5.4543×10^{-2} (4.33×10^{-3})
	4	**3.8807×10^{-1} (2.84×10^{-2})**	5.4492×10^{-1} (2.64×10^{-2})	7.2794×10^{-1} (1.93×10^{-2})	4.2046×10^{-1} (1.84×10^{-2})	4.3567×10^{-1} (4.43×10^{-2})	4.7314×10^{-1} (4.87×10^{-2})
	6	**$1.0007 (4.60 \times 10^{-2})$**	$1.1423 (7.05 \times 10^{-2})$	$1.2727 (1.71 \times 10^{-1})$	$1.1062 (5.67 \times 10^{-2})$	$1.1087 (7.63 \times 10^{-2})$	$1.2195 (3.66 \times 10^{-2})$
	8	$1.9327 (1.18 \times 10^{-1})$	$1.8850 (8.85 \times 10^{-2})$	$2.5821 (4.74 \times 10^{-1})$	**$1.8000 (1.06 \times 10^{-1})$**	$1.9315 (1.84 \times 10^{-1})$	$1.9155 (1.66 \times 10^{-1})$
	10	$2.7443 (8.17 \times 10^{-2})$	**$2.5220 (9.52 \times 10^{-2})$**	5.9788 (1.56)	$2.7594 (1.55 \times 10^{-1})$	$2.7525 (2.04 \times 10^{-1})$	$3.6191 (5.42 \times 10^{-1})$
WFG8	3	4.1394×10^{-2} (5.07×10^{-3})	1.0573×10^{-1} (2.93×10^{-2})	1.1245×10^{-1} (1.01×10^{-2})	5.8739×10^{-2} (3.21×10^{-3})	**2.9373×10^{-2} (2.97×10^{-3})**	3.0148×10^{-2} (4.10×10^{-3})
	4	4.8901×10^{-1} (8.06×10^{-3})	6.4358×10^{-1} (1.46×10^{-1})	7.3375×10^{-1} (1.27×10^{-1})	4.6162×10^{-1} (3.81×10^{-2})	**3.9637×10^{-1} (4.15×10^{-2})**	4.1740×10^{-1} (1.89×10^{-2})
	6	$1.1665 (4.24 \times 10^{-2})$	$1.2605 (1.27 \times 10^{-1})$	$1.6225 (2.73 \times 10^{-1})$	$1.1242 (2.69 \times 10^{-2})$	$1.1578 (6.09 \times 10^{-2})$	**$1.0230 (1.80 \times 10^{-2})$**
	8	$2.0692 (1.43 \times 10^{-1})$	$2.1098 (7.91 \times 10^{-2})$	$3.0526 (3.64 \times 10^{-1})$	$2.0188 (1.14 \times 10^{-1})$	$1.9674 (1.60 \times 10^{-1})$	**$1.8048 (4.19 \times 10^{-2})$**
	10	$3.1190 (1.07 \times 10^{-1})$	$3.2001 (6.82 \times 10^{-2})$	6.0940 (1.05)	$3.0400 (7.18 \times 10^{-2})$	**$2.8524 (2.39 \times 10^{-1})$**	$2.8567 (9.21 \times 10^{-2})$
WFG9	3	4.2924×10^{-2} (2.18×10^{-2})	6.0561×10^{-2} (1.18×10^{-2})	7.3145×10^{-2} (1.54×10^{-2})	**3.0844×10^{-2} (3.90×10^{-3})**	5.5430×10^{-2} (1.95×10^{-2})	5.5138×10^{-2} (1.56×10^{-2})
	4	5.1027×10^{-1} (4.90×10^{-2})	6.1318×10^{-1} (3.12×10^{-2})	7.2063×10^{-1} (9.47×10^{-2})	4.4146×10^{-1} (4.96×10^{-2})	**4.3061×10^{-1} (2.27×10^{-2})**	4.4446×10^{-1} (7.10×10^{-2})
	6	$1.1379 (1.18 \times 10^{-1})$	$1.2651 (1.61 \times 10^{-1})$	$1.5483 (1.98 \times 10^{-1})$	$1.0847 (6.09 \times 10^{-2})$	$1.0492 (2.88 \times 10^{-2})$	**9.5946×10^{-1} (2.10×10^{-2})**
	8	$1.8927 (6.59 \times 10^{-2})$	$2.0609 (7.48 \times 10^{-2})$	$2.8191 (1.95 \times 10^{-1})$	$2.0055 (8.54 \times 10^{-2})$	**$1.7157 (1.13 \times 10^{-1})$**	$1.7858 (2.36 \times 10^{-1})$
	10	$2.9128 (2.02 \times 10^{-1})$	$2.7467 (2.33 \times 10^{-1})$	$6.6172 (7.72 \times 10^{-1})$	$2.8216 (1.52 \times 10^{-1})$	**$2.3043 (2.07 \times 10^{-1})$**	$2.7752 (1.00 \times 10^{-1})$

Table A2
IGD mean and standard deviation of each algorithm on DTLZ test set

Problem	M	ABSAEA	ADSAPSO	CPSMOEA	PCSAEA	PBRVEA	KG_HSEA
DTLZ1	3	2.5421×10^{1} (3.67)	**9.0385 (5.58)**	1.0562×10^{1} (9.19)	9.1497 (8.52)	1.4304×10^{1} (4.29)	1.8795×10^{1} (3.52)
	4	4.2109×10^{1} (1.25)	5.7676×10^{1} (3.57×10^{1})	5.4299×10^{1} (2.63×10^{1})	**2.4853×10^{1} (1.56)**	3.2647×10^{1} (2.81)	3.3104×10^{1} (7.94)
	6	**1.1845×10^{1} (3.80)**	4.7418×10^{1} (2.20×10^{1})	4.0666×10^{1} (1.10×10^{1})	1.9115×10^{1} (1.17×10^{1})	2.1070×10^{1} (1.01×10^{1})	1.9133×10^{1} (3.66)
	8	2.1739×10^{1} (1.09×10^{1})	2.4353×10^{1} (6.26)	4.4457×10^{1} (1.14×10^{1})	2.1624×10^{1} (1.03)	**1.0560×10^{1} (6.88)**	1.4177×10^{1} (3.09)
	10	2.2281×10^{1} (6.68)	3.2526×10^{1} (2.02×10^{1})	4.0208×10^{1} (2.56×10^{1})	2.4670×10^{1} (6.90)	**1.2627×10^{1} (4.96)**	1.4189×10^{1} (2.50)
DTLZ2	3	1.4690×10^{-1} (1.11×10^{-1})	1.1907×10^{-1} (4.04×10^{-2})	1.6192×10^{-1} (7.17×10^{-2})	2.6244×10^{-1} (2.02×10^{-2})	1.1595×10^{-1} (2.45×10^{-2})	**7.1394×10^{-2} (2.25×10^{-2})**
	4	1.9975×10^{-1} (2.29×10^{-2})	3.6047×10^{-1} (6.38×10^{-2})	5.3392×10^{-1} (1.80×10^{-2})	2.5937×10^{-1} (1.40×10^{-2})	1.4657×10^{-1} (7.88×10^{-3})	**1.3484×10^{-1} (5.52×10^{-3})**
	6	3.1693×10^{-1} (2.79×10^{-2})	4.1928×10^{-1} (2.95×10^{-2})	6.8733×10^{-1} (7.45×10^{-2})	3.9067×10^{-1} (2.10×10^{-2})	**2.6849×10^{-1} (4.98×10^{-3})**	2.7181×10^{-1} (6.51×10^{-3})
	8	4.2368×10^{-1} (9.93×10^{-3})	5.6024×10^{-1} (3.36×10^{-2})	8.7977×10^{-1} (3.45×10^{-2})	5.5287×10^{-1} (3.94×10^{-2})	3.8899×10^{-1} (4.90×10^{-3})	**3.7538×10^{-1} (9.58×10^{-3})**
	10	4.7017×10^{-1} (5.64×10^{-3})	5.4937×10^{-1} (3.87×10^{-2})	7.2872×10^{-1} (2.21×10^{-2})	**4.4817×10^{-1} (8.24×10^{-3})**	4.6925×10^{-1} (1.55×10^{-3})	5.1306×10^{-1} (2.33×10^{-2})
DTLZ3	3	2.7984×10^{2} (1.95)	2.5536×10^{2} (1.51×10^{2})	**6.6217×10^{1} (5.72×10^{1})**	2.4713×10^{2} (4.76×10^{1})	2.6499×10^{2} (1.92×10^{1})	1.4728×10^{2} (7.99)
	4	1.1040×10^{2} (4.93×10^{1})	1.3194×10^{2} (3.35×10^{1})	1.0123×10^{2} (3.22×10^{1})	9.9653×10^{1} (2.77×10^{1})	**9.8986×10^{1} (2.56×10^{1})**	1.0633×10^{2} (1.79×10^{1})
	6	6.4357×10^{1} (3.15×10^{1})	1.1901×10^{2} (5.53×10^{1})	1.3323×10^{2} (3.50×10^{1})	4.4961×10^{1} (2.94)	**2.7434×10^{1} (1.97×10^{1})**	4.9965×10^{1} (1.00×10^{1})
	8	1.3770×10^{1} (8.61)	2.3964×10^{1} (1.17×10^{1})	3.2281×10^{1} (1.22×10^{1})	**8.8487 (2.30)**	1.9309×10^{1} (8.58)	1.4438×10^{1} (6.84)
	10	**7.6229×10^{-1} (6.54×10^{-2})**	1.2209 (7.38×10^{-1})	1.2728×10^{1} (1.11×10^{1})	1.2033 (4.85×10^{-1})	8.4166×10^{-1} (7.94×10^{-2})	2.1239 (2.04)
DTLZ4	3	2.6203×10^{-1} (8.82×10^{-2})	4.9663×10^{-1} (1.47×10^{-1})	**2.2991×10^{-1} (5.27×10^{-2})**	4.4017×10^{-1} (2.13×10^{-2})	4.5156×10^{-1} (3.17×10^{-1})	6.6840×10^{-1} (2.98×10^{-1})
	4	3.2829×10^{-1} (2.92×10^{-2})	5.3508×10^{-1} (1.95×10^{-2})	6.0907×10^{-1} (4.62×10^{-2})	4.3401×10^{-1} (8.32×10^{-2})	**2.5716×10^{-1} (1.06×10^{-1})**	6.8054×10^{-1} (8.39×10^{-2})
	6	4.8110×10^{-1} (2.16×10^{-2})	5.4416×10^{-1} (4.24×10^{-2})	6.6550×10^{-1} (4.69×10^{-2})	4.8886×10^{-1} (2.44×10^{-2})	**3.7777×10^{-1} (3.89×10^{-2})**	9.3334×10^{-1} (3.77×10^{-1})
	8	6.1814×10^{-1} (3.07×10^{-2})	6.7801×10^{-1} (3.48×10^{-2})	7.3407×10^{-1} (1.70×10^{-2})	5.8329×10^{-1} (1.77×10^{-2})	**5.6614×10^{-1} (5.68×10^{-2})**	1.6594 (2.91×10^{-1})
	10	6.3812×10^{-1} (1.08×10^{-2})	6.9926×10^{-1} (5.51×10^{-2})	7.8362×10^{-1} (1.24×10^{-2})	**5.3903×10^{-1} (1.46×10^{-2})**	6.2585×10^{-1} (6.77×10^{-2})	1.4312 (4.40×10^{-1})
DTLZ5	3	1.2754×10^{-1} (3.46×10^{-2})	1.0237×10^{-1} (2.53×10^{-2})	1.7165×10^{-1} (4.14×10^{-2})	8.8365×10^{-2} (1.30×10^{-2})	2.8133×10^{-2} (6.69×10^{-3})	**1.3101×10^{-2} (2.27×10^{-3})**
	4	3.8513×10^{-2} (7.05×10^{-3})	2.1286×10^{-1} (5.47×10^{-2})	2.0879×10^{-1} (2.64×10^{-2})	8.5393×10^{-2} (1.13×10^{-2})	**2.8746×10^{-2} (6.16×10^{-3})**	4.6595×10^{-2} (1.12×10^{-2})
	6	3.2800×10^{-2} (6.72×10^{-3})	1.4410×10^{-1} (2.60×10^{-2})	2.5562×10^{-1} (8.40×10^{-2})	8.7686×10^{-2} (6.12×10^{-3})	**2.1919×10^{-2} (3.91×10^{-3})**	7.8734×10^{-2} (3.06×10^{-2})
	8	**2.0740×10^{-2} (8.18×10^{-3})**	7.4926×10^{-2} (1.03×10^{-2})	1.5695×10^{-1} (4.53×10^{-2})	5.2676×10^{-2} (1.10×10^{-2})	2.4519×10^{-2} (7.84×10^{-3})	5.7099×10^{-2} (2.25×10^{-2})
	10	**6.0048×10^{-3} (3.57×10^{-4})**	2.1079×10^{-2} (1.14×10^{-3})	1.9919×10^{-1} (1.02×10^{-1})	1.0756×10^{-2} (7.19×10^{-4})	2.7387×10^{-2} (6.40×10^{-3})	1.8561×10^{-2} (2.82×10^{-3})
DTLZ6	3	3.8895 (2.42×10^{-1})	4.1340 (2.66)	3.9716 (9.57×10^{-2})	5.7959 (2.90×10^{-1})	4.1125 (2.75×10^{-1})	**1.8062 (5.18×10^{-1})**
	4	1.7170 (7.76×10^{-1})	4.6089 (5.03×10^{-1})	2.5004 (7.80×10^{-1})	4.8435 (3.07×10^{-1})	1.8849 (3.23×10^{-1})	**1.3114 (3.59×10^{-1})**
	6	1.1805 (1.03×10^{-1})	2.4223 (4.58×10^{-1})	1.9243 (4.34×10^{-1})	3.5608 (1.21×10^{-1})	1.3790 (2.02×10^{-1})	**7.6824×10^{-1} (1.69×10^{-1})**
	8	1.5885 (8.41×10^{-1})	3.4667 (4.30×10^{-1})	2.6009 (6.54×10^{-1})	3.6407 (5.85×10^{-2})	1.3365 (1.24×10^{-1})	**6.1612×10^{-1} (4.28×10^{-1})**
	10	9.9369×10^{-2} (2.15×10^{-2})	5.4376 (1.48×10^{-1})	4.3252 (1.90×10^{-1})	9.7530×10^{-2} (8.68×10^{-2})	5.7298×10^{-2} (1.79×10^{-3})	**3.5360×10^{-2} (3.61×10^{-3})**
DTLZ7	3	4.3253×10^{-1} (3.69×10^{-1})	5.6069 (8.85×10^{-1})	6.8055 (1.32)	4.2848 (5.91×10^{-1})	2.1928×10^{-1} (1.94×10^{-2})	**1.4992×10^{-1} (2.38×10^{-2})**
	4	4.8597×10^{-1} (1.41×10^{-1})	5.3673 (6.79×10^{-1})	2.0747 (1.35)	3.0848 (8.63×10^{-1})	**2.1842×10^{-1} (8.54×10^{-3})**	2.3525×10^{-1} (9.01×10^{-2})
	6	1.2052 (2.93×10^{-1})	2.7352 (1.32)	1.6676 (2.15×10^{-1})	3.7156 (2.14)	**4.3140×10^{-1} (6.87×10^{-2})**	5.8744×10^{-1} (3.09×10^{-1})
	8	1.3163 (6.47×10^{-2})	7.1511 (7.25)	2.4033 (3.13×10^{-1})	7.1313 (9.46×10^{-1})	1.2062 (2.65×10^{-1})	**8.7904 $\times 10^{-1}$ (3.24×10^{-1})**
	10	1.2431 (6.27×10^{-2})	1.6958 (1.88×10^{-1})	1.8570 (6.53×10^{-2})	1.4057 (6.37×10^{-2})	1.3368 (1.46×10^{-1})	**9.3437 $\times 10^{-1}$ (1.15×10^{-1})**